eTransportation 9 (2021) 100120

Contents lists available at ScienceDirect

eTransportation

journal homepage: www.journals.elsevier.com/etransportation

A comparison of various universally applicable power distribution strategies for fuel cell hybrid trains utilizing component modeling at different levels of detail: From simulation to test bench measurement☆

Hujun Peng [a, *], Zhu Chen [a], Kai Deng [a], Steffen Dirkes [b], Cem Ünlübayir [c], Andreas Thul [a], Lars Löwenstein [d], Dirk Uwe Sauer [c], Stefan Pischinger [b], Kay Hameyer [a]

[a] RWTH Aachen University, Institute of Electrical Machines (IEM), Germany
[b] RWTH Aachen University, Institute for Combustion Engines (VKA), Germany
[c] RWTH Aachen University, Institute for Power Electronics and Electrical Drives (ISEA), Chair for Electrochemical Energy Conversion and Storage Systems, Germany
[d] Siemens Mobility GmbH, Vienna, Austria

ARTICLE INFO

Article history:
Received 8 March 2021
Received in revised form
24 April 2021
Accepted 18 May 2021
Available online 25 May 2021

Keywords:
Fuel cell hybrid vehicles
Scalable energy management strategies
APMP
Experimental measurement

ABSTRACT

A comparative study of energy management strategies for fuel cell hybrid trains, which focuses merely on universally applicable power distribution strategies, is presented in this contribution. These scalable strategies include a load follower strategy, an adaptive rule-based strategy, and adaptive Pontryagin's minimum principle (APMP)-based strategies with or without considering the relaxation process in batteries. For the load follower strategy, information about the characteristic consumption curves of the fuel cell system and the equivalent circuit of the batteries is not required. The adaptive rule-based strategy exploits the fuel cell system's characteristic consumption curves to maintain the fuel cell power close to its mean value. For the APMP-based strategies, in addition to the fuel cell modeling, the battery modeling with and without relaxation process in batteries is considered separately. In order to fairly compare the different scalable energy management strategies regarding hydrogen efficiency, Pontryagin's minimum principle-based strategy is used as the reference strategy, which considers the relaxation process in batteries. The comparison of the four strategies in terms of fuel economy is firstly based on the simulative analysis. For the different strategies, the additional hydrogen consumption amounts to 1.6%, 0.7%, 0.6%, and 0.6% respectively, compared to the reference strategy under a typical all-day regional train driving cycle. Then, in the RWTH Aachen University's Center for Mobile Propulsion, the hydrogen consumption is measured experimentally using the different strategies for a short driving cycle. The APMP strategy considering the relaxation process in batteries, consumes the least hydrogen per kilometer travel of 161.9 g/km, with charge sustaining maintained, which is the most energy-efficient energy management strategy. The simulation and experimental results show that the strategy should be selected based on the level of detail to utilize the modeling accuracy of components. Furthermore, due to the scalability of the strategies, they can be further transferred to other applications without enormous tuning effort.

© 2021 Elsevier B.V. All rights reserved.

1. Introduction

1.1. Background

Using hydrogen technology to reduce carbon dioxide emissions attract more and more attention. The European Commission presented its hydrogen strategy to meet the 2050 climate neutrality

☆ This research is funded by the German Federal Ministry of Transport and Digital Infrastructure (BMVi), with the funding numbers of 03B10502B and 03B10502B2.

* Corresponding author.
E-mail address: hujun.peng@iem.rwth-aachen.de (H. Peng).

https://doi.org/10.1016/j.etran.2021.100120
2590-1168/© 2021 Elsevier B.V. All rights reserved.

goal of the European Green Deal last year [1]. In order to reduce emissions in transportation, hydrogen-powered vehicles, buses, and trains have already become a reality. Toyota brought the second generation of fuel cell hybrid vehicles *Mirai* to market in 2020 [2]. Numerous companies have carried hydrogen fuel cell studies and practical fuel cell bus trials [3]. Alstom's first fuel cell hybrid trains began their commercial service in Germany in 2017. In December 2020, the train completed its three months of testing in Austria. So far, a total number of 41 fuel cell trains of Alstom have been sold [4]. Siemens is also developing fuel cell trains based on its platform *Mireo*. A joint project is carried on with Ballard Power System and RWTH Aachen University to investigate the interaction between fuel cell systems and batteries [5]. Recently, Siemens and Deutsche Bahn announced to launch fuel cell trains trial [6]. This contribution results from the project with Siemens and the strategies to be introduced can be transferred to other applications.

1.2. Literature survey

As there are two energy sources available and no extra chargers in the fuel cell hybrid trains, power distribution between fuel cells and batteries is controlled to improve fuel economy and durability and safety of components [7]. In Ref. [8], various degradation modeling methods of fuel cells and batteries are reviewed. In Ref. [9], battery thermal safety is considered in developing energy management strategies for hybrid vehicles with a high energy battery system and a high power battery system. The energy management strategies are commonly grouped in three types, including rule-based strategies, optimization-based strategies, and learning-based strategies [10,11]. In Ref. [12], different energy management strategies are reviewed for battery and capacitor hybrid systems regarding energy efficiency and battery aging. In Ref. [13], the power allocation strategies are comparatively studied for fuel cell and capacitor hybrid vehicles. However, the local optimization-based methods are not comprehensively discussed in Ref. [13]. The principles of various strategies and their advantages as well as drawbacks can be found in many works. In the following parts, the rule-based methods, including deterministic and fuzzy logic-based rule strategies, the local optimization-based method including various sub-types, and the global optimization-based method, and the learning-based method, are sequentially reviewed based on literature study.

The rule-based strategy can be divided into deterministic and fuzzy logic rules. The deterministic rules contain PI-controller, finite state machine, load follower, frequency separation, or combining these common strategies [14]. The rule-based strategy has a low computational load, which is suitable for real-world applications. Nevertheless, its performance regarding fuel efficiency is limited because the expert experience, which is the basis of the rule-based strategy, is restricted. In Ref. [15], genetic algorithms are applied in energy management strategies to optimize rules, parameters, and objectives. But, the genetic algorithm is more suitable for parameter optimization than process optimization, and predefined driving cycles are necessary. In Ref. [16], the strategy uses a low-pass filter to determine the hybrid ship's fuel cell power. The cut-off frequency varies based on the support vector machine to identify the ship's operation conditions. However, the support vector machine needs to be trained offline, which limits its adaptivity. In Ref. [17], a finite state machine is used as energy management considering the batteries and fuel cells' power capability. Thereby, various control rules based on heuristic experiences are developed. Nevertheless, the fuel cell systems are frequently turned on and off, not desired in practical applications. In Ref. [18], state machine, operational mode control, and equivalent consumption minimization strategy (ECMS) are combined with utilizing their advantages. Numerous parameters are introduced to classify the vehicle state, battery and fuel cell operation, and load power demand into various scenarios. But, as learned from the results, the fuel cell power system is often turned on and off, which shortens its lifetime and the total fuel efficiency. Furthermore, a comparison to optimal offline strategies is not given. In Ref. [19], the charge depletion and charge sustaining strategy's threshold values are optimized based on convex programming. However, the threshold values resulted from convex programming also limit their scalability to other vehicle configurations.

In terms of the fuzzy rule-based strategy, various membership functions must be determined for the fuzzy variables. The membership functions' parameters can be optimized using a genetic algorithm to improve fuel economy under certain driving conditions [20]. However, the optimized membership function does not maintain its effectiveness under other driving conditions. In order to improve the performance of the fuzzy rule-based controller under different driving conditions, in Ref. [20], a self-organizing map is trained to classify driving patterns. Under each driving pattern, a corresponding fuzzy rule-based controller is optimized offline by using evolutionary algorithms.

The optimization-based strategies include local and global ones. The local optimization-based method is an online strategy, and the most famous ones include the ECMS, the adaptive Pontryagin's minimum principle-based strategy (APMP), and the model predictive controller (MPC), or a combination of them. In Ref. [21], it is proved that the ECMS is mathematically related to APMP. In Ref. [22], damping factors are added to the Hamiltonian to penalize the fuel cell power fluctuation. Thereby, the lifetime cost is reduced with a slight hydrogen consumption increase. However, the costate value is assumed to be constant, which is identified to vary in the offline results. As the degradation of components during operation increases, the local optimization-based method should also consider the actual component characteristics [7]. In Ref. [23], a forgetting factor recursive least square method is used to identify the maximum efficiency range of the actual fuel cell systems, and this information is integrated into an optimized ECMS. However, the resulted fuel cell power experiences high fluctuation, from which the total energy efficiency and the lifetime suffer. In Ref. [24], the fuel cell model used in the APMP-based energy management is updated according to the degradation degree of fuel cells to get a higher hydrogen efficiency over the whole lifetime, which indicates the dependency of the costate on the characteristic curve of components. However, quantitatively adjusting the costate in function degradation degree is not plausibly derived. In order to improve the adaptivity, driving pattern recognition technology can be integrated into the APMP-based strategy. In Ref. [25], a support vector machine is used to realize online recognition, which is trained based on existing data using particle swarm optimization. Under each driving pattern, a constant costate value is assumed, which is not optimal. The MPC strategy minimizes predefined cost function with various constraints on control and state variables considered. In Ref. [26], the MPC controller reduces fuel cell power fluctuation and maintains SoC and temperature constraints. In the cost function, various weighting factors are introduced to balance different goals. However, these factors are tuned manually, limiting the applications under other situations. In Ref. [27], the predictive model controller aims at minimizing hydrogen consumption and component degradation. Thereby, the cost function is not a linear or quadratic form of the control variable. Therefore, dynamic programming is adopted to determine the control sequences. However, the choice of the weighting factors, which are included in the cost function, remains challenging. In Ref. [28], the Markov speed forecast mechanism is used to predict future load power. Moreover, based on the historical trip information, a reference trajectory for

SoC is generated. Finally, a multi-objective controller is developed by introducing various weighting factors. However, the weighting factors are not generally optimal for other driving conditions. In order to avoid using weighting factors in the cost function [29], introduces an APMP-based MPC algorithm to minimize the total equivalent hydrogen consumption in the time horizon. Thereby, the costate is accurately estimated by the formula described in Ref. [30].

Regarding the global optimization-based method, the most famous strategies are Pontryagin's minimum principle (PMP) as well as dynamic programming. In Ref. [31], implementation of both algorithms with relaxation process in batteries considered are comprehensively introduced. They can provide accurate and fair references for comparing online energy management strategies, which is not the case for most existing works relating to a comparative study of energy management strategies.

Regarding the learning-based strategy, the control law is derived from massive training data using a data mining algorithm [32]. In Ref. [33], ECMS based on reinforcement learning is developed. Thereby, in the definition of the total equivalent hydrogen consumption, various weighting factors penalize individual components' unbeneficial operations. However, a vast data set collected for three years is used to tune these parameters, influencing the strategy's scalability if another vehicle is to be controlled instead of the trained ones.

Summarily, the reviewed energy management strategies found in the literature do not show enough transferability or scalability. Various crucial factors are defined in the strategies, such as the weighting factors in MPC or parameters defined in the rule-based strategy. These factors are not physically derived but based on heuristic experience, which can be further tuned by using offline results or training data. However, the effectiveness is then limited to cases similar to the training data. Therefore, most reviewed works about energy management for fuel cell hybrid vehicles concentrate on the strategies that lack scalability and optimality when implemented. A comparative study that only focuses on scalable strategies has not been found in the studies.

1.3. Main work

In order to solve the problem of scalability faced with energy management, model-based strategies were developed and introduced in our previous work. In Ref. [34], the convexity of the fuel cell system's specific consumption curve is used to maintain the fuel cell system operating around its mean value and realize high fuel efficiency and prolong fuel cell lifetime. In this way, the degradation of fuel cells as well as the fuel efficiency are not contradictory any more. Furthermore, in Ref. [30], an analytical formula to calculate the costate in APMP is derived by using the state of charge (SoC) of the battery system and the mean value of fuel cell power for hydrogen-powered vehicles. As the formula is model-based, the actual component characteristics are self-explanatory considered. Furthermore, the APMP strategy is more promising than ECMS because of the physically derived formula. Then, the APMP strategy's robustness against component aging is validated in Ref. [35]. However, the relaxation process in batteries is not considered in the implementation of APMP, which will be further developed in this work. Moreover, with various scalable strategies available, the choice of the most suitable strategy becomes essential. However, a comprehensive comparison between different scalable strategies is lacking. Therefore, the following contributions are made to address the void:

- The scalable APMP will be further developed with the relaxation process in batteries considered, which utilizes more accurate modeling than the existing one. As the most precise modeling of batteries and fuel cells is used in the APMP strategy, the hydrogen efficiency is the highest. Under a typical whole-day driving cycle, the fuel cell hybrid trains with this strategy used consume merely 0.6% more hydrogen than optimal offline strategies.
- Simulative and experimental analyses are carried out for four different scalable strategies, including load follower, which outputs fuel cell power dependent on the SoC level, the adaptive rule-based strategy, and the APMP strategies considering the relaxation process in batteries or not. It is worth mentioning that the test bench has a peak power of one Megawatt, which is the testbed with the highest power rating in the world so far, to analyze the fuel cell and battery hybrid system.
- Offline PMP with the relaxation process in batteries considered is implemented to evaluate the performance of the scalable strategies mentioned above, which is a fair and accurate reference. Compared to other literature, which also comparatively studies different strategies, the reference strategies used here are more precise, making the comparison more convincing.

1.4. Outline of the paper

The whole modeling of the fuel cell hybrid trains, which is required for analyzing the fuel economy, is shortly displayed in section 2. Then, the offline PMP considering relaxation processes in the battery system is briefly described in section 3. After that, four scalable strategies are introduced in section 4. Next, an analysis of the strategies by using simulations is given in section 5. Then, the experimental measurement is introduced in section 6. Finally, a short conclusion and outlook will be given in section 7.

2. Driveline

The configuration of the total driveline is shown in Fig. 1. The auxiliary power consumption, in which the air condition makes a big part, is assumed to be 30 kW in summer. In this work, the whole system is modeled in Simulink. Its structure is displayed in Fig. 2, and the power demand of a half train is modeled. In Fig. 2, the F_{demand} stands for the force demand from drivers, P_{demand} is the auxiliary power consumption, F_{traction} is the traction force, F_{brake} is the mechanical braking force, v_{train} is the train velocity, and F_{normal} represents the component force of gravity in the vertical direction. Besides the dynamical calculation of the battery SoC and the train velocity, other subsystems are modeled by using lookup tables. The detailed modeling and parameters of each subsystem in the driveline are described in Ref. [34]. The speed and altitude profiles of several train lines are implemented in the simulation, as displayed in Fig. 3. Fig. 3a shows the speed trajectory of the railway section between Mannheim, Karlsruhe and Basel. The second figure displays the round trip of Regional Express 1 from Aachen to Cologne, and then back to Aachen. And Fig. 3c shows the trajectory of the regional train RE27 running through Berlin and Brandenburg.

2.1. Fuel cell systems

In the project, the polymer electrolyte membrane (PEM) fuel cells are utilized, which are chosen due to their high power density, high system efficiency, quick start-up, good behavior under high dynamic as well as zero-emission. The utilized fuel cell system consists of two parallel-connected stacks and other ancillary components in coolant, air as well as hydrogen paths. The net

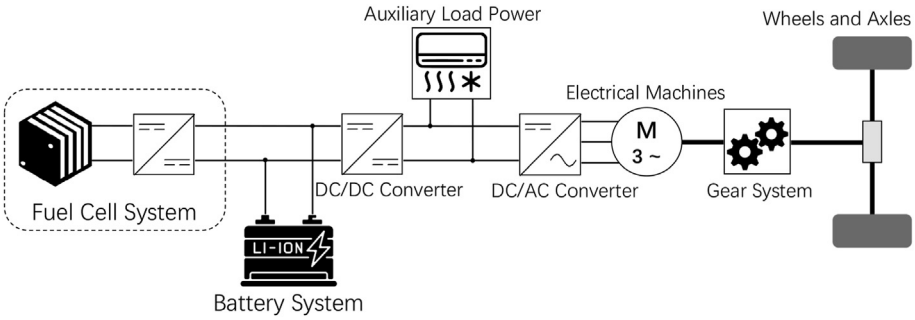

Fig. 1. Configuration of the driveline.

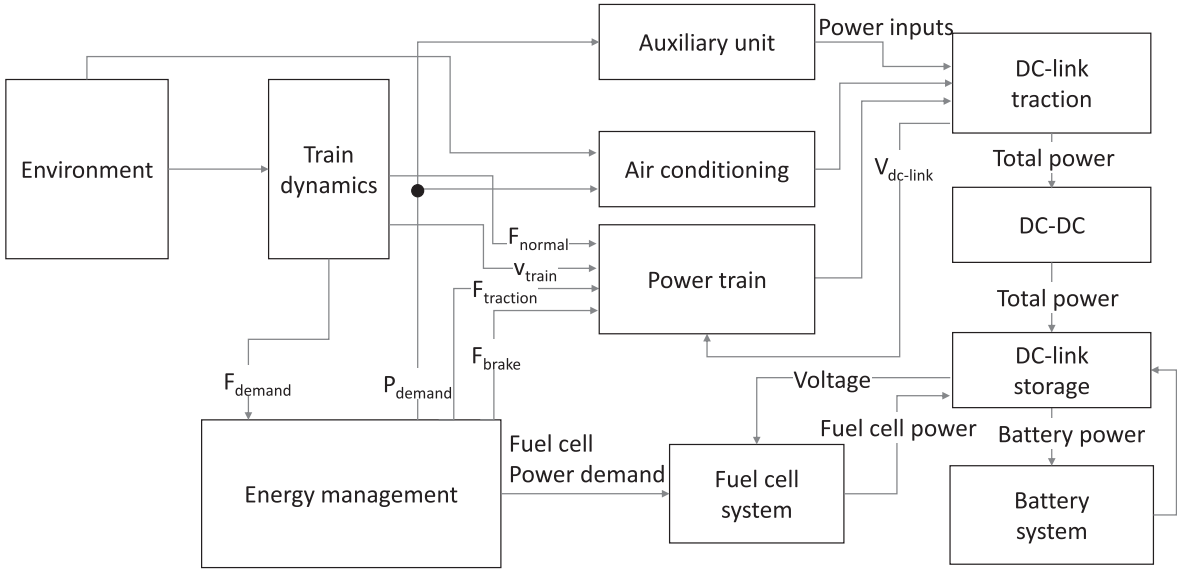

Fig. 2. Schematic signal flow between subsystems of the fuel cell hybrid train.

maximum power of the fuel cell system is 200 kW. Fig. 4 shows the entire fuel cell system's characteristic consumption curve. Moreover, the characteristic consumption curve of degraded fuel cell systems of the same product is also displayed as a comparison.

As a precondition of using the PMP-based strategy to determine optimal offline results, the hydrogen consumption curve's convexity within the operating range is required. Fig. 5 shows the convexity of the characteristic consumption curve of the fuel cell system, which corresponds to the following equation:

$$\dot{m}_{H_2}(\alpha \cdot P_{fc,\,1} + (1-\alpha) \cdot P_{fc,\,2}) < \alpha \cdot \dot{m}_{H_2}(P_{fc,\,1}) + (1-\alpha) \cdot \dot{m}_{H_2}(P_{fc,\,2}), \quad (1)$$

where $\dot{m}_{H_2}$ stands for the mass flow, which is a function of the fuel cell system's net output power, α is a number between 0 and 1, and $P_{fc,\,1}$ and $P_{fc,\,2}$ are two arbitrarily selected operation points of the fuel cell system.

2.2. Configuration of the lithium-titanate-oxide battery system

Due to the long lifetime of the lithium-titanate-oxide (LTO) battery cells, they are applied in the fuel cell hybrid train. The equivalent electrical circuit with three resistor-capacitor parallel branches is adopted to model the entire battery system in Fig. 6, which differs from most literature. As a result, the voltage drops due to the entire internal resistance and relaxation processes can be modeled accurately. As the active cooling is implemented in the simulation, the temperature change of the battery systems is neglected. The dependency of the open-circuit voltage, as well as the inner resistance R_0 on the SoC, are measured, as displayed in Fig. 7a and Fig. 7b, respectively. Fig. 7c–h displays the parasitic resistors and the various time constants in function of SoC, fitted by measurement data. The total capacity of the battery system is around 200 kWh, and its rated voltage is 835 V.

3. Offline PMP with the relaxation process in batteries considered

In this section, a PMP-based offline strategy is introduced, which provides an accurate global optimal solution. Thus, this offline strategy can be further utilized as a benchmark to compare other online strategies in the next section. The detailed information about the offline PMP strategy can be found in Ref. [35], and here, merely the important equations are reviewed.

Before the implementation of the strategy, the following variables and parameters are defined. The SoC of the battery is defined as the state variable, and the output power of the fuel cell systems is selected as the control variable. The three voltages over the parasitic resistor-capacitor branches are treated as changeable parameters, represented by V_1, V_2, and V_3, respectively. Thus, only the SoC can be controlled freely, and the same battery current couples the parasitic voltages over the parallel branches. As the hydrogen consumption is to be minimized, the Hamiltonian function, which

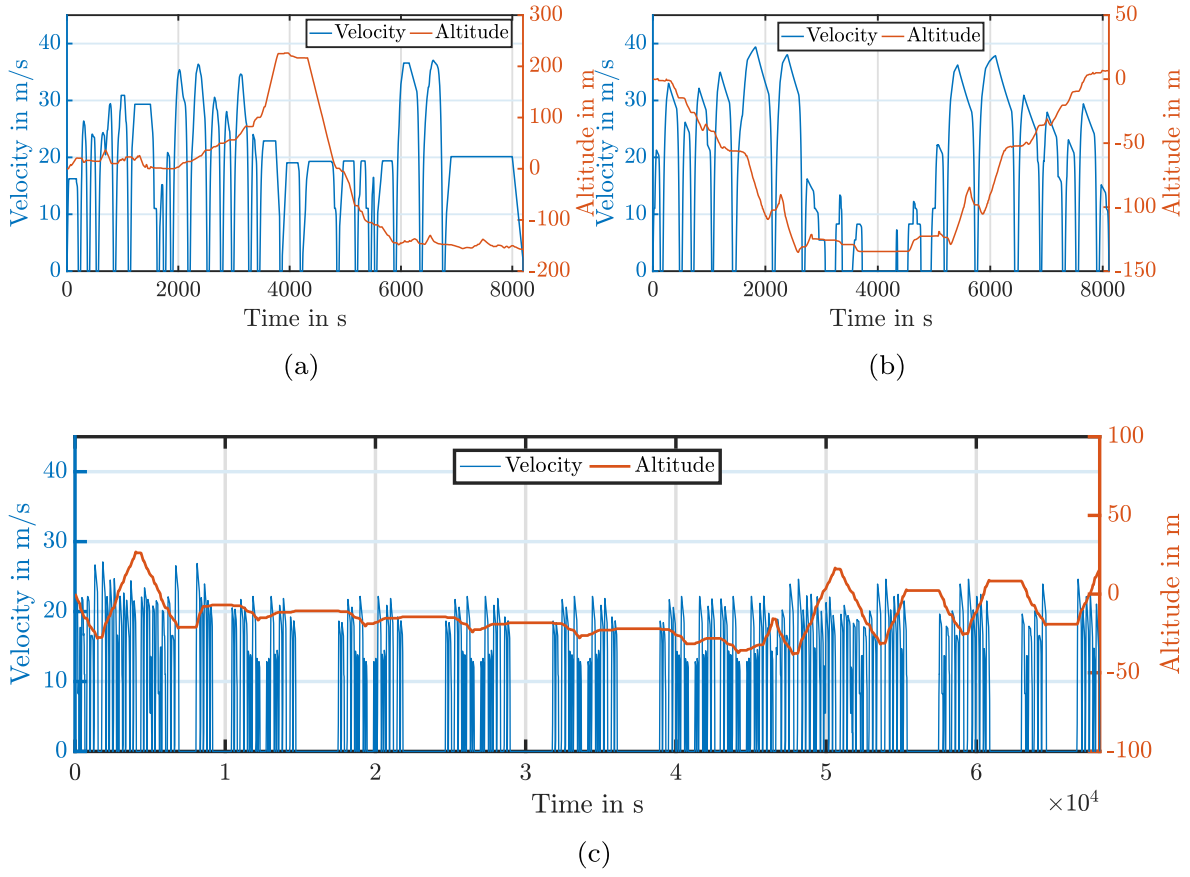

Fig. 3. The driving cycles: (a) A: between Mannheim, Karlsruhe and Basel (b) B: between Aachen and Cologne (c) C: through Berlin and Brandenburg.

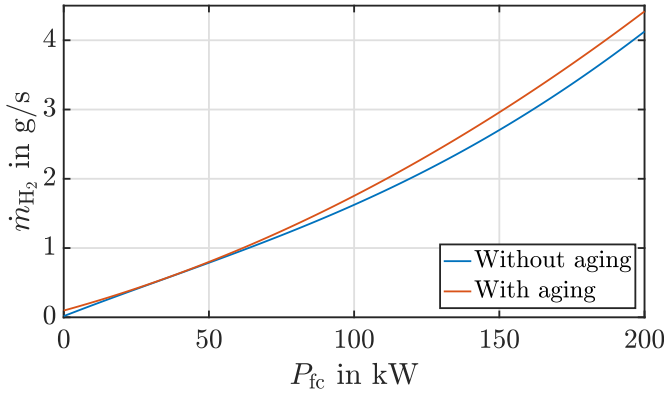

Fig. 4. Characteristic consumption curves of fuel cell systems with and without aging.

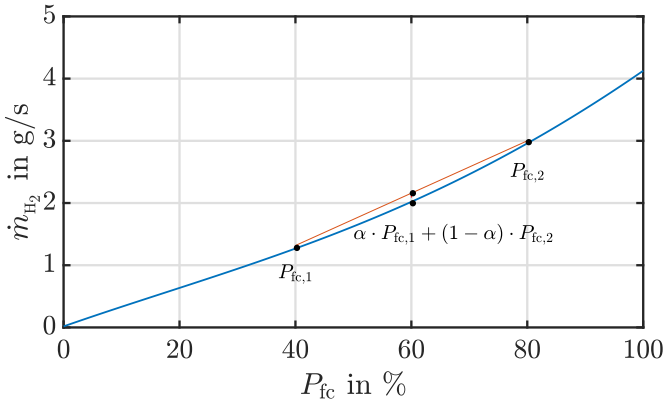

Fig. 5. Characteristic consumption of the fuel cell system in function of output power and its convexity.

is the core part of the PMP-based strategy, is defined as follows:

$$H(SoC(t), P_{fc}(t), \lambda(t), t) = \dot{m}_{H_2}(P_{fc}(t)) + \lambda(t) \cdot \dot{SoC}(t), \tag{2}$$

whereby $\dot{m}_{H_2}$ stands for the mass flow of hydrogen, which depends on the output power of the fuel cell system, and $\lambda(t)$ is the costate. Then, the optimal control variable is found with the following equation:

$$P^*_{fc}(t) = \arg\min_{P_{fc}(t)} \left(H(SoC(t), P_{fc}(t), \lambda(t), t)\right), \tag{3}$$

in order to minimize the Hamiltonian function H in each time

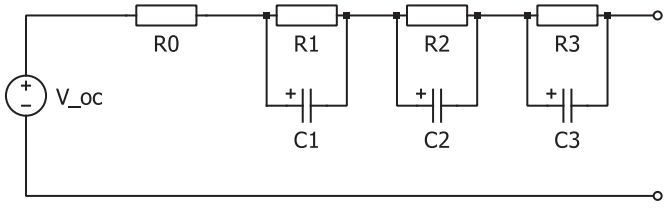

Fig. 6. The equivalent electrical circuit of the battery system.

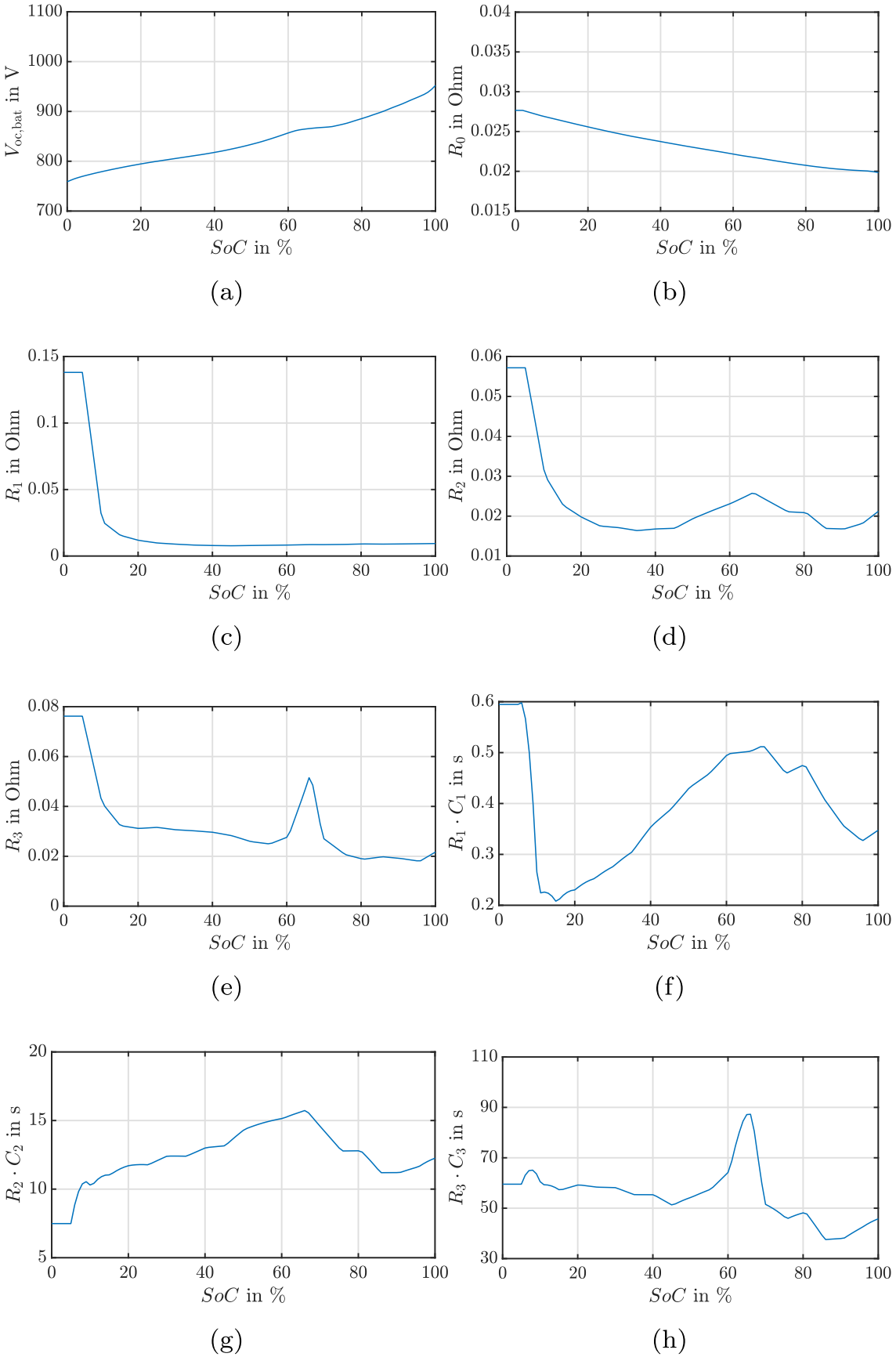

Fig. 7. Dependency of the battery system's equivalent electrical circuit parameters on SoC: (a) The open-circuit voltage $V_{oc,\ bat}$ in Volt, (b) R_0, (c) R_1, (d) R_2, (e) R_3, (f) The time constant $R_1 \cdot C_1$ in seconds, (g) $R_2 \cdot C_2$ in seconds, (h) $R_3 \cdot C_3$ in seconds.

instant. In the following, the dynamic of the SoC and the costate λ will be derived.

Firstly, another variable V_{diff} is used to describe the difference between the battery system's open-circuit voltage and the sum of various parasitic voltages:

$$V_{\text{diff}} = V_{\text{oc, bat}} - V_1 - V_2 - V_3. \tag{4}$$

Then, the battery system output power is formulated as follows:

$$P_{\text{bat}} = I_{\text{bat}} \cdot (V_{\text{diff}} - R_{0,\text{ bat}} \cdot I_{\text{bat}}) = P_{\text{load}} - P_{\text{fc}}. \tag{5}$$

Furthermore, the entire battery system current is written by using the output power of the fuel cell system as well as the load power:

$$I_{\text{bat}} = \frac{V_{\text{diff}}}{2R_{0,\text{ bat}}} - \frac{\sqrt{(V_{\text{diff}})^2 - 4(P_{\text{load}} - P_{\text{fc}})R_{0,\text{ bat}}}}{2R_{0,\text{ bat}}}. \tag{6}$$

As the parasitic voltages are included in V_{diff}, the dynamics of the parasitic voltages can be calculated with the battery current as follows:

$$\begin{cases} \dot{V}_1 &= -\dfrac{V_1}{R_1 \cdot C_1} + \dfrac{1}{C_1} \cdot I_{\text{bat}}, \\ \dot{V}_2 &= -\dfrac{V_2}{R_2 \cdot C_2} + \dfrac{1}{C_2} \cdot I_{\text{bat}}, \\ \dot{V}_3 &= -\dfrac{V_3}{R_3 \cdot C_3} + \dfrac{1}{C_3} \cdot I_{\text{bat}}, \end{cases} \tag{7}$$

where R_1, R_2, R_3 and C_1, C_2, C_3 are the parasitic resistances and capacitances, all of which depend on SoC of the battery system. Based on (6), the dynamic of the SoC can be determined:

$$\dot{SoC}(t) = -\frac{V_{\text{diff}}}{2R_{0,\text{ bat}}Q_{\text{bat}}} + \frac{\sqrt{(V_{\text{diff}})^2 - 4(P_{\text{load}} - P_{\text{fc}})R_{0,\text{ bat}}}}{2R_{0,\text{ bat}} \cdot Q_{\text{bat}}}. \tag{8}$$

Then, in the following, the dynamic of the costate will be derived. As mentioned before, SoC is the only state variable, and the parasitic voltages are defined as changeable parameters. Therefore, the partial derivatives of these changeable parameters to SoC are equal to zero. Based on that, the dynamic of the costate variable can be derived as follows:

$$\dot{\lambda} = -\lambda \cdot \frac{\partial \dot{SoC}}{\partial SoC} = -\lambda \cdot \left(\frac{\partial \dot{SoC}}{\partial V_{\text{oc, bat}}} \cdot \frac{\partial V_{\text{oc, bat}}}{\partial SoC} + \frac{\partial \dot{SoC}}{\partial R_{0,\text{ bat}}} \cdot \frac{\partial R_{0,\text{ bat}}}{\partial SoC} \right) \tag{9}$$

The partial derivative of the battery system's SoC change rate with respect to $V_{\text{oc, bat}}$ and $R_{0,\text{ bat}}$ are determined by the following equations:

$$\frac{\partial \dot{SoC}}{\partial V_{\text{oc, bat}}} = -\frac{1}{2R_{0,\text{ bat}}Q_{\text{bat}}} \cdot \left(1 - \frac{V_{\text{diff}}}{\sqrt{V_{\text{diff}}^2 - 4(P_{\text{load}} - P_{\text{fc}})R_{0,\text{ bat}}}} \right), \tag{10}$$

$$\frac{\partial \dot{SoC}}{\partial R_{0,\text{ bat}}} = \frac{1}{2R_{0,\text{ bat}}^2 Q_{\text{bat}}} \left(\frac{2(P_{\text{load}} - P_{\text{fc}})R_{0,\text{ bat}} - V_{\text{diff}}^2}{\sqrt{V_{\text{diff}}^2 - 4(P_{\text{load}} - P_{\text{fc}})R_{0,\text{ bat}}}} + V_{\text{diff}} \right) \tag{11}$$

As the sequence of load power is given as an input, the optimal control variable can be found with (3). Then, the state and costate variables are updated for the next time instant by using equations (8) and (9), whereby (7) is used to determine the V_{diff} in (8), while (10) and (11) are utilized to calculate the (9). After an iterative calculation until the final time instant, the sequences of the fuel cell system power, as well as the SoC under the optimal control, are determined, with which the hydrogen consumption is minimized.

In the next section, various online energy management strategies will be introduced. As mentioned in the literature review, the offline PMP strategy can be used as a reference strategy. For that purpose, it is worth mentioning that for comparison, the load power trajectory and the SoC start and end values, which result from online strategies, will be used as input to run the offline PMP algorithm. In other words, each online strategy's performance will be separately compared to its corresponding offline results.

4. Universally online applicable strategies

In this section, the principle of four different universally applicable strategies will be introduced. The universality means that no crucial parameters, which have to be tuned for different driving cycles or system configurations, are introduced in the strategies. Therefore, the strategies can be transferred to other applications and systems without tuning effort.

4.1. Load follower maintaining SoC at middle level

According to the load follower strategy, the output power of the fuel cell system follows the load power change to keep the battery SoC at the middle level. Thereby, the output power of fuel cell system is determined according to a control curve, as depicted in Fig. 8. The fuel cell systems output maximum power if the SoC is lower than 50%. Above 50%, the output power of the fuel cell system decreases linearly as the SoC increases. If SoC is larger than 90%, the fuel cell system is turned off to avoid overcharging the batteries. The threshold values related to the strategy, including the slope of decrease, can be optimized for each specific driving cycle. Here, the value 50% and 90% are coarsely determined, and further optimization is not the target of this contribution and therefore not considered.

If the load power increases, as happens during the acceleration phase, the battery system assists the acceleration by providing high positive power, and the battery SoC decreases. According to the control strategy, fuel cell power begins to increase. After the acceleration phase, the load power demand decreases, which is smaller than the output power of the fuel cell systems. Then, the excess fuel cell power charges the battery system, and the SoC returns to a balanced value. While in the regenerative braking

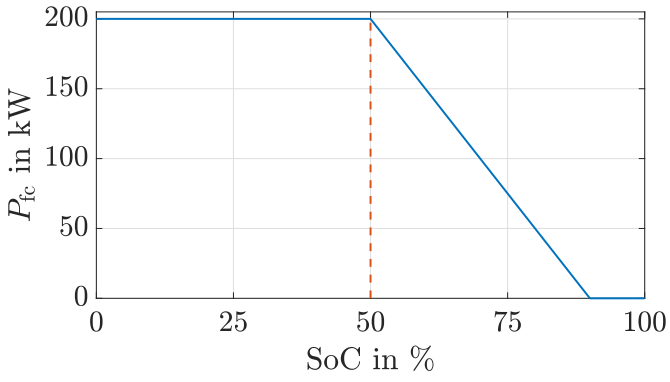

Fig. 8. Mechanism of the load follower strategy.

phase, the load power is negative, and the SoC increases. As the SoC increased, the fuel cell system outputs less power to avoid overcharging of batteries, and the SoC begins to go back to its balance value.The most important advantage lies in its robustness and low computational effort. No information about component modeling is necessary. If the component ages with time, the control strategy retains its effectiveness, because merely SoC is required to control the fuel cell power instead of other component-related parameters. As a result, the output power of the fuel cell systems oscillates around the mean load power due to the trains' various operation phases, from which the fuel economy and the fuel cell lifetime suffer. This drawback will be solved by introducing an adaptive rule-based method utilizing the fuel cell system's characteristic consumption curve's convexity in the next subsection.

4.2. Adaptive rule-based strategies utilizing the characteristic consumption curves of fuel cell systems

In section 2.1, the convexity of the fuel cell system's characteristic consumption curve is explained. According to the convexity, the hydrogen efficiency can be improved when the output power of the fuel cell systems is near its mean value. For a given train travel, this principle can be described by using the following equation:

$$\dot{m}_{H_2}(P_{fc}) < \frac{\int_0^T \dot{m}_{H_2}(P_{fc}(\tau))\, d\tau}{T}, \tag{12}$$

whereby T stands for the travel time and τ is the instant time.

When the charge-sustaining condition is satisfied, the load side's total energy demand should be fully supplied by the fuel cell system. Here, the battery losses due to inner resistance are neglected. Then, the charge-sustaining condition can be expressed by using the following equation:

$$\int_0^T P_{fc}(\tau)d\tau = \int_0^T P_{load}(\tau)d\tau. \tag{13}$$

Thus, according to (12), if the operating points of the fuel cell system are concentrated and are close to the global average of the load power, a better hydrogen efficiency results. In this subsection, the design of an adaptive rule-based strategy based on this principle is introduced. Its mechanism is shown in Fig. 9a.In the case of a low SoC level, the fuel cell system is controlled to work in mode 1, in which the fuel cell power increases to be $(1+a)$ times of the load power average value, whereby a is a positive factor. Conversely, in the case of a high SoC level, the fuel cell system works in mode 3 and its power is decreased by factor b. Otherwise, the fuel cell systems work in mode 2, and its power equals the average load power. Furthermore, in order to avoid frequent transition between

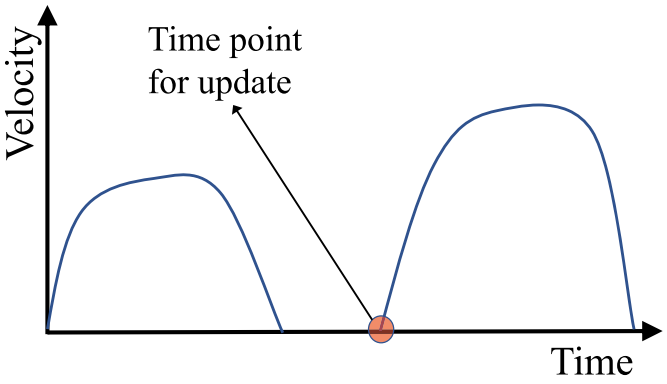

Fig. 10. Schematic explaining the time point to renew the mean value of the load power.

different modes, a hysteresis control is implemented in Fig. 9b, which helps to reduce oscillation in fuel cell power. In this contribution, the switch points of the SoC $a1$, $a2$, $a3$, $a4$ are set to 0.25, 0.35, 0.85 and 0.95, respectively. For a higher fuel efficiency, the train should work in mode 2 as much as possible. Thus, the calculation of the load power average value becomes a crucial task in this strategy.

In online applications, the load power's global average value during the whole travel is unknown in advance. Hence, the average load power is estimated based on historical information. The load power demand of a train has massive variations in three phases: acceleration, cruising and regenerative breaking. During the acceleration, the power demand is massive to overcome the inertia force. In this case, the average load power could be overestimated. Conversely, as the load power is negative during regenerative breaking, the average load power could be underestimated. In order to reduce estimation error, the average load power update occurs every time the train leaves stations instead of during driving between two stations. Fig. 10 shows the time point in which the load power average value is calculated and updated. Besides, the detailed process of calculating the average load power is introduced in Ref. [34].

4.3. APMP without considering the relaxation process in batteries

In the offline PMP strategy, the optimal initial value of the costate is determined with a shooting method. Thereby, the load information along the entire driving cycle is required, which is not possible in real-time applications. In this section, an adaptive PMP-based strategy is introduced as an online strategy. For this purpose, an analytical formula is introduced to regularly correct the costate by using history information to keep the online strategy casual. According to the energy conservation principle, the costate value

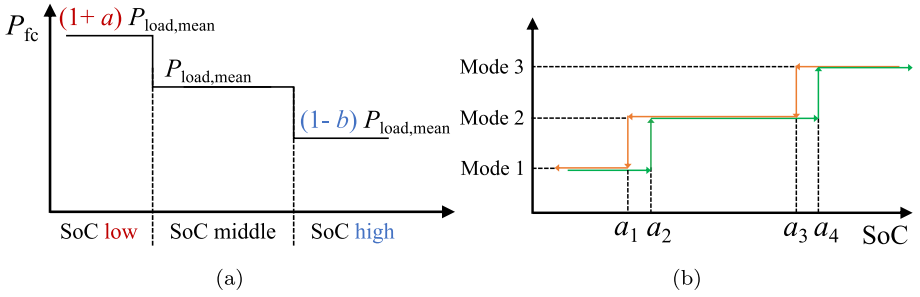

Fig. 9. Mechanism of the adaptive rule-based strategy: (a) Three operation modes, (b) Mode transition with the help of the hysteresis control.

depicts the equivalent hydrogen mass of using the battery power, as the battery discharging now has to be compensated by consuming hydrogen in the future. The costate is identified as a function of SoC and the fuel cell system's average power. The detailed derivation and description of the function can be found in Ref. [30]. Here, only the most important steps of deriving the analytical formula are introduced.

In (3), the optimal control of the Hamiltonian function is chosen. Thus, it can be assumed that the partial derivative of the Hamiltonian function with respect to the output power of the fuel cell system at the optimal control value equals zero:

$$\left.\frac{\partial H}{\partial P_{\mathrm{fc}}}\right|_{P_{\mathrm{fc}}=P_{\mathrm{fc}}^{*}}=\left.\frac{\partial \dot{m}_{\mathrm{H_2}}}{\partial P_{\mathrm{fc}}}+\lambda\cdot\frac{\partial \dot{SoC}}{\partial P_{\mathrm{fc}}}\right|_{P_{\mathrm{fc}}=P_{\mathrm{fc}}^{*}}=0, \tag{14}$$

where P_{fc}^{*} is the optimal fuel cell power that minimizes the Hamiltonian function. Due to the convexity of the fuel cell system's consumption curve, the optimal control approximately equals the global mean value of the fuel cell system power. Thus, (14) can be rewritten by substituting the average value:

$$\left.\frac{\partial H}{\partial P_{\mathrm{fc}}}\right|_{P_{\mathrm{fc}}=\overline{P}_{\mathrm{fc}}}=\left.\frac{\partial \dot{m}_{\mathrm{H_2}}}{\partial P_{\mathrm{fc}}}+\lambda\cdot\frac{\partial \dot{SoC}}{\partial P_{\mathrm{fc}}}\right|_{P_{\mathrm{fc}}=\overline{P}_{\mathrm{fc}}}=0. \tag{15}$$

Thereby, the derivative of the battery SoC's change rate with respect to the output power of the fuel cell systems can be derived from (8) as:

$$\frac{\partial \dot{SoC}}{\partial P_{\mathrm{fc}}}=\frac{1}{Q_{\mathrm{bat}}}\cdot\frac{1}{\sqrt{V_{\mathrm{oc,\,bat}}^{2}-4\cdot(P_{\mathrm{load}}-P_{\mathrm{fc}})R_{0,\,\mathrm{bat}}}}. \tag{16}$$

It deserves mentioning that instead of V_{diff} in (8), $V_{\mathrm{oc,\,bat}}$ is used because the parasitic resistance-capacitor branches are not considered in the APMP here. By substituting (16) into (15), the costate can be calculated with:

$$\lambda=-\left.\frac{\partial \dot{m}_{\mathrm{H_2}}}{\partial P_{\mathrm{fc}}}\cdot\left(Q_{\mathrm{bat}}\cdot\sqrt{V_{\mathrm{oc,\,bat}}^{2}-4\cdot\left(P_{\mathrm{load}}-P_{\mathrm{fc}}\right)\cdot R_{0,\,\mathrm{bat}}}\right)\right|_{P_{\mathrm{fc}}=\overline{P}_{\mathrm{fc}}}. \tag{17}$$

Within this equation, the derivative of the hydrogen mass flow to the output power of the fuel cell system depends on the P_{fc}, as displayed in Fig. 11, and the $V_{\mathrm{oc,\,bat}}$ and $R_{0,\,\mathrm{bat}}$ are functions of SoC, as depicted in Fig. 7a and b, respectively.Since the mean power value

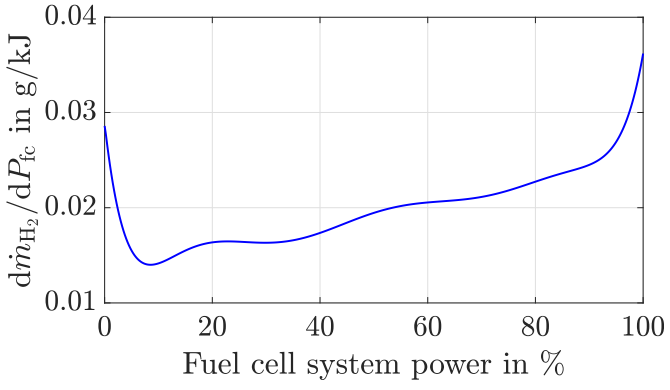

Fig. 11. The derivative of the hydrogen mass flow to the output power of the fuel cell systems.

of the fuel cell system almost equals the load demand power's global average value, the term with $R_{0,\,\mathrm{bat}}$ in (17) could be neglected. Then, the analytical calculation of the costate can be written as:

$$\lambda=-\left.\frac{\partial \dot{m}_{\mathrm{H_2}}}{\partial P_{\mathrm{fc}}}\cdot Q_{\mathrm{bat}}\cdot V_{\mathrm{oc,\,bat}}\right|_{P_{\mathrm{fc}}=\overline{P}_{\mathrm{fc}}}, \tag{18}$$

which displays the costate λ as a function of the mean power of the fuel cell system as well as the battery open-circuit voltage or rather SoC. In Fig. 12, the analytically estimated costate values are compared to the offline strategy's results. Under various combinations of battery SoC and mean power values of the fuel cell system, resulting from simulations under all the three driving cycles, the costate's analytical estimation overlaps with the offline trajectory to a large degree. Therefore, the correctness of the analytical formula in Eq. (18) is validated.

In implementing the APMP strategy, the costate value is regularly corrected by using this formula to eliminate the strategy's sensitivity to the costate. The costate value is renewed with the analytical formula every time the train leaves a station, which is similar to the previous section's rule-based strategy. During the remaining time, except leaving up stations, the costate is updated by using (9) to utilize the optimal control theory. It is worth mentioning that V_{diff} in (10) and (11) is replaced by $V_{\mathrm{oc,\,bat}}$, because the parasitic voltages are not considered here.

Besides, the fuel cell system's mean power values along the entire drive cycles are unknown in real-time applications. Therefore, the load power demand and the loss power in batteries in the past are utilized to estimate fuel cell system power's mean values. It worths mentioning that accurately estimating the mean power is easy to implement if GPS and communication technology are used.

4.4. APMP with the relaxation process in batteries considered

In this subsection, the APMP strategy is further improved by considering the parasitic resistance/capacitor branches. Identical to the offline PMP part, the dynamics of costate and SoC are updated with (8) and (9), respectively, whereby the parasite voltages are considered, as required in (10) and (11). The regular correction of the costate with the analytical formula is the same as in the previous subsection 4.3. It has to be mentioned that the battery management system does not provide the parasitic voltages. Therefore, they will be calculated inside the energy management system, as the resistance and capacitance in batteries are determined with lookup tables since displayed in Fig. 7c–h. Then, the corresponding parasitic voltages are updated with (7). With the relaxation process considered, the high accuracy of the battery modeling is utilized.

5. Simulation results

5.1. Simulation results of load follower

Fig. 13 shows the output power trajectories of the fuel cell systems as well as the battery SoC for different driving cycles. These trajectories are compared to the offline PMP strategy's optimal results, which are determined under the same load power trajectory and battery SoC end value. The resulted battery SoC trajectories remain within a relatively small range. It is more evident in the result under the driving cycle C, as presented in Fig. 13e, and the other two driving cycles are too short-time to show this phenomenon clearly. Since the control variable depends purely on the battery SoC, the output power of the fuel cell systems jumps to the upper limit when the initial SoC value of the battery system is less

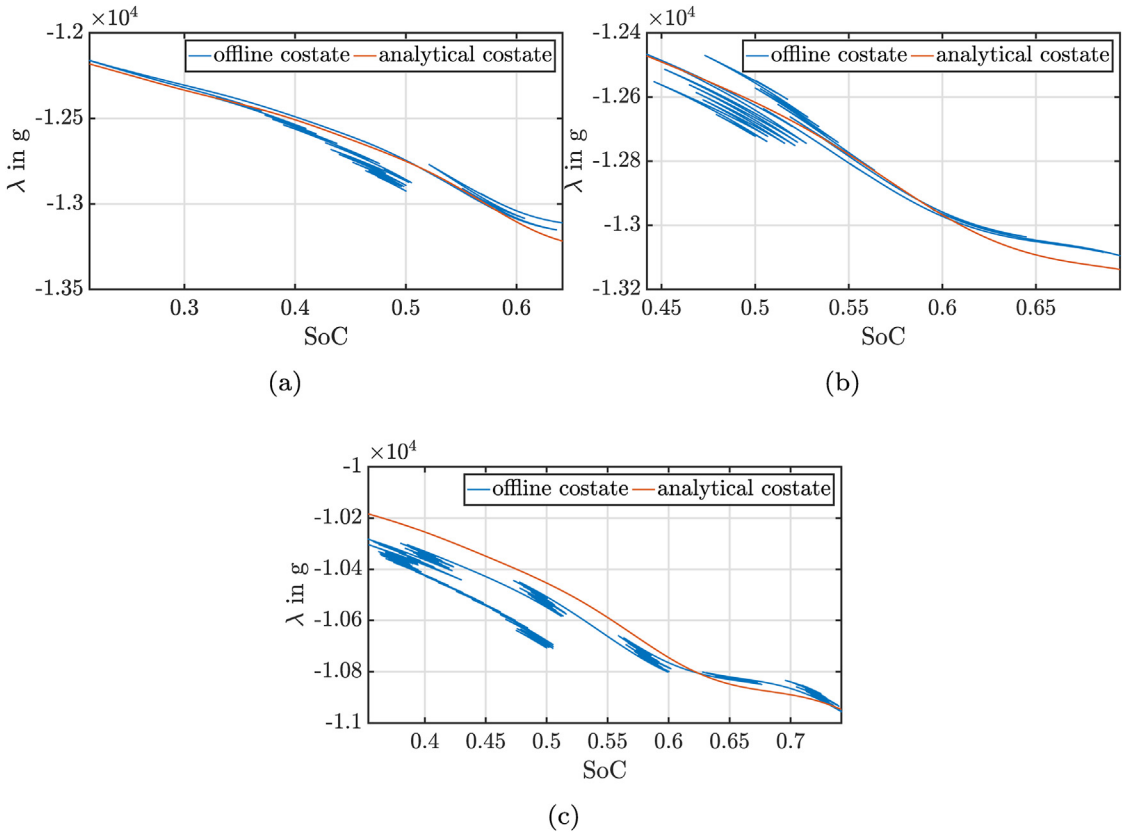

Fig. 12. Analytically calculated costate values based on the battery SoC at the average output power of the fuel cell system under various driving cycles, which are compared to the offline results: (a) A driving cycle with P_{fc} equal to 106.5 kW, (b) B driving cycle with P_{fc} equal to 114.1 kW, (c) C driving cycle with P_{fc} equal to 78.5 kW.

than 0.5. As presented in Fig. 13a, c and 13e, the fuel cell power trajectories have a strong vibration, which reduces the hydrogen usage efficiency according to the fuel cell system's characteristic consumption curve. This drawback is more obvious under the two short driving cycles A and B, and their hydrogen consumption values are 7.7% and 4.2% higher than that of the offline strategy, as displayed in Table 1.

5.2. Simulation results under the adaptive rule-based strategy

The output power trajectories of the fuel cell systems under the adaptive rule-based strategy and the corresponding offline results are displayed in Fig. 14a, c and e. As the fuel cell system power's mean values are renewed at each railway stop, the trajectories have a stepped form. In Fig. 14a, the fuel cell power raises rapidly at around 4000 s. The reason is that the SoC gets close to the lower limit, and the fuel cell power is adjusted to avoid over-discharging. As the sequence under driving cycle C in Fig. 14e shows, the fuel cell power maintains around an average value, which is similar to its corresponding offline results. Furthermore, the SoC trajectories under the rule-based strategy are almost overlapped with the SoC trajectories under the offline results, as shown in Fig. 14b, d and f. Thus, the fuel economy of the adaptive rule-based strategy is relatively high compared to the load follower. Its hydrogen consumption is 3.1%, 1.6%, and 0.7% higher than the optimal solution under each driving cycle.

5.3. Simulation results of APMP strategy

Compared to the adaptive rule-based strategy, the output power trajectories of the fuel cell systems under the APMP strategy show more oscillation due to its principle. However, the fuel cell power lies in a relatively small range around the offline sequences, as displayed in Fig. 15a, c and e. Under driving cycle C, the deviation of the fuel cell power trajectories from the corresponding offline results is the smallest. The reason for that lies in the much longer driving time of the driving cycle C, which provides more historical information records so that the error in estimating costate values is less than under other driving cycles. The slightly more significant deviations under driving cycles A and B are caused by the over-and underestimation of the fuel cell system's mean output power. However, the negative and positive deviations compensate against each other so that the charge-sustaining condition is not influenced overly. In Fig. 16, the costate variable's trajectories are displayed. The costate trajectory under driving cycle C also shows a higher degree of coincidence with the corresponding offline result due to high accuracy in estimating the costate. As for the SoC trajectories, they strongly overlap with the their corresponding offline results, as displayed in Fig. 15b, d and f. Compared to the corresponding offline results, the resulting additional hydrogen consumption is 2.2%, 1.5%, and 0.6% for different driving cycles, respectively, which is further improved compared to the adaptive, scalable rule-based strategy (see Table 2).

5.4. Simulation results of APMP with the relaxation process in batteries considered

In this subsection, by considering the parasitic capacitor/resistance branches, the APMP strategy is further improved. The corresponding fuel cell system's power and the SoC trajectories are shown in Fig. 17. They overlap with the corresponding offline results to a large degree. In order to show the influence of considering

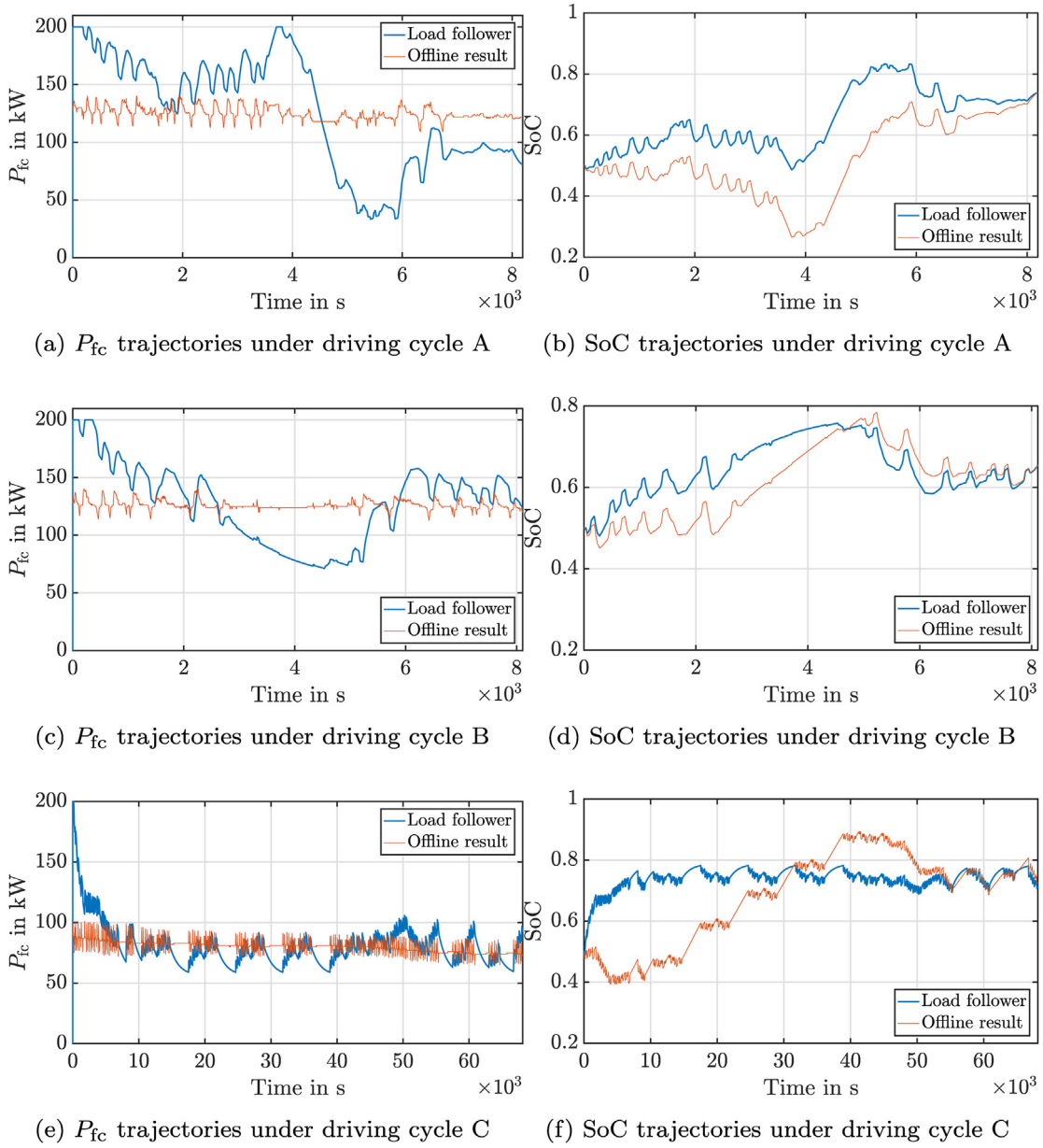

Fig. 13. SoC and fuel cell power trajectories under the load follower strategy, compared to offline results.

Table 1
Simulation results of load follower.

Driving cycle	A	B	C
P_{fc}	126.06	127.1	80.98
SoC_{end}	0.739	0.655	0.726
m_{H_2} (g)	37514	36346	177220
Offline m_{H_2} (g)	34818	34892	174512
Ref. m_{H_2}	7.7 %	4.2 %	1.6 %
m_{H_2} (g/km)	243.4	249.2	303.2

Table 2
Simulation results under the adaptive rule-based strategies.

Driving cycles	A	B	C
P_{fc}	118.85	116.15	78.18
SoC_{end}	0.637	0.512	0.403
m_{H_2} (g)	33074	31590	168972
Offline m_{H_2} (g)	32080	31086	167816
Ref. m_{H_2}	3.1 %	1.6 %	0.7 %
m_{H_2} (g/km)	214.6	216.6	289

the relaxation process in batteries in the APMP, the trajectories are plotted together with the results under the APMP strategy without considering the relaxation process in Fig. 18. Thereby, a slight difference can be observed, and a further improvement in the fuel efficiency results. The additional hydrogen consumption compared to the corresponding offline results under driving cycle A and B are reduced from 2.2% and 1.5% to 2.1% and 1.4%, respectively, while that under the driving cycle C keeps the value of 0.6%. The resulted data of the APMP strategies with and without considering the relaxation process in batteries are listed in Table 3.

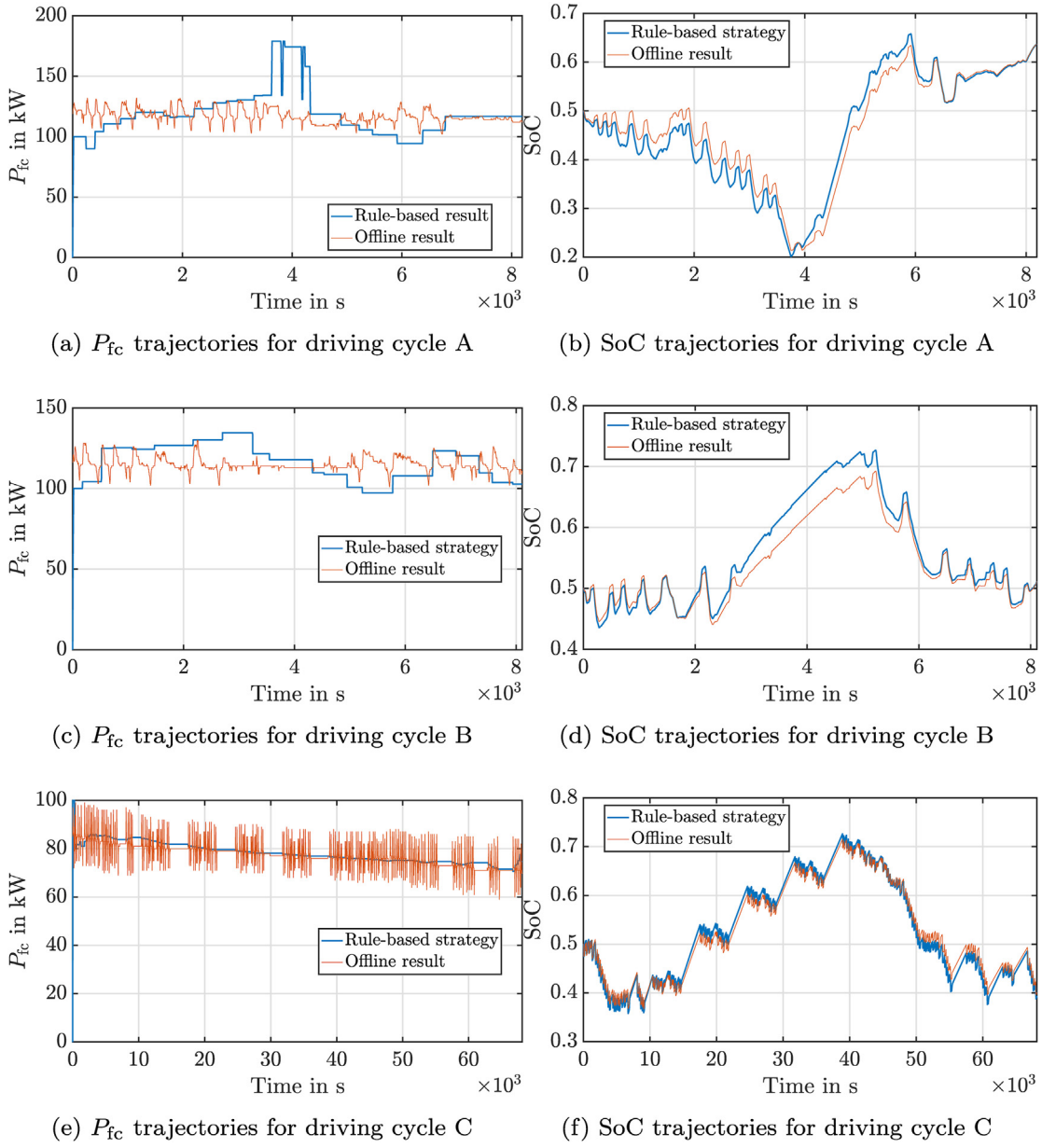

Fig. 14. SoC and fuel cell power trajectories under the adaptive rule-based strategies, compared to offline results.

5.5. Comparison of four strategies

Fig. 19a, c and e show the resulted fuel cell power sequences of four introduced strategies. The P_{fc} of load follower has a huge vibration to maintain its SoC within a narrower range. However, this leads to a drawback in the fuel economy, and the buffer function of the battery systems is not fully utilized. The trajectories under the other three strategies have a similar form, as they are all based on calculating the load power's mean value. A rapid change of fuel cell power can be observed in the adaptive rule-based strategy for the driving cycle A, which prevents the SoC from falling below its boundary-value. As for the SoC trajectories of all strategies, they are compared with each other in Fig. 19b, d and f. The load follower's SoC trajectory is quite different from the others. It maintains a narrower range, especially under the driving cycle C. The resulting SoC trajectories of the other three strategies are almost overlapped and achieve the charge-sustaining condition. For the hydrogen efficiency, by comparing the hydrogen consumption in Table 4, the rule-based strategy and the APMP strategies are proved to be more hydrogen efficient than the load follower strategy. Thereby, the fuel cell system's characteristic consumption curve's convexity is considered in the adaptive rule-based strategy to improve hydrogen consumption efficiency. The APMP strategy further enhances the fuel economy compared to the adaptive rule-based strategies by quantitatively utilizing the battery and fuel cell modeling. Finally, the APMP strategy with the relaxation process in batteries considered provides an even better result than the APMP strategy without considering the relaxation process.

6. Experimental validation

6.1. Test bench configuration

Fig. 20 shows the structure of the test bench at RWTH Aachen University to validate the hydrogen efficiency of various strategies. There are two energy resources: a fuel cell system with a derated

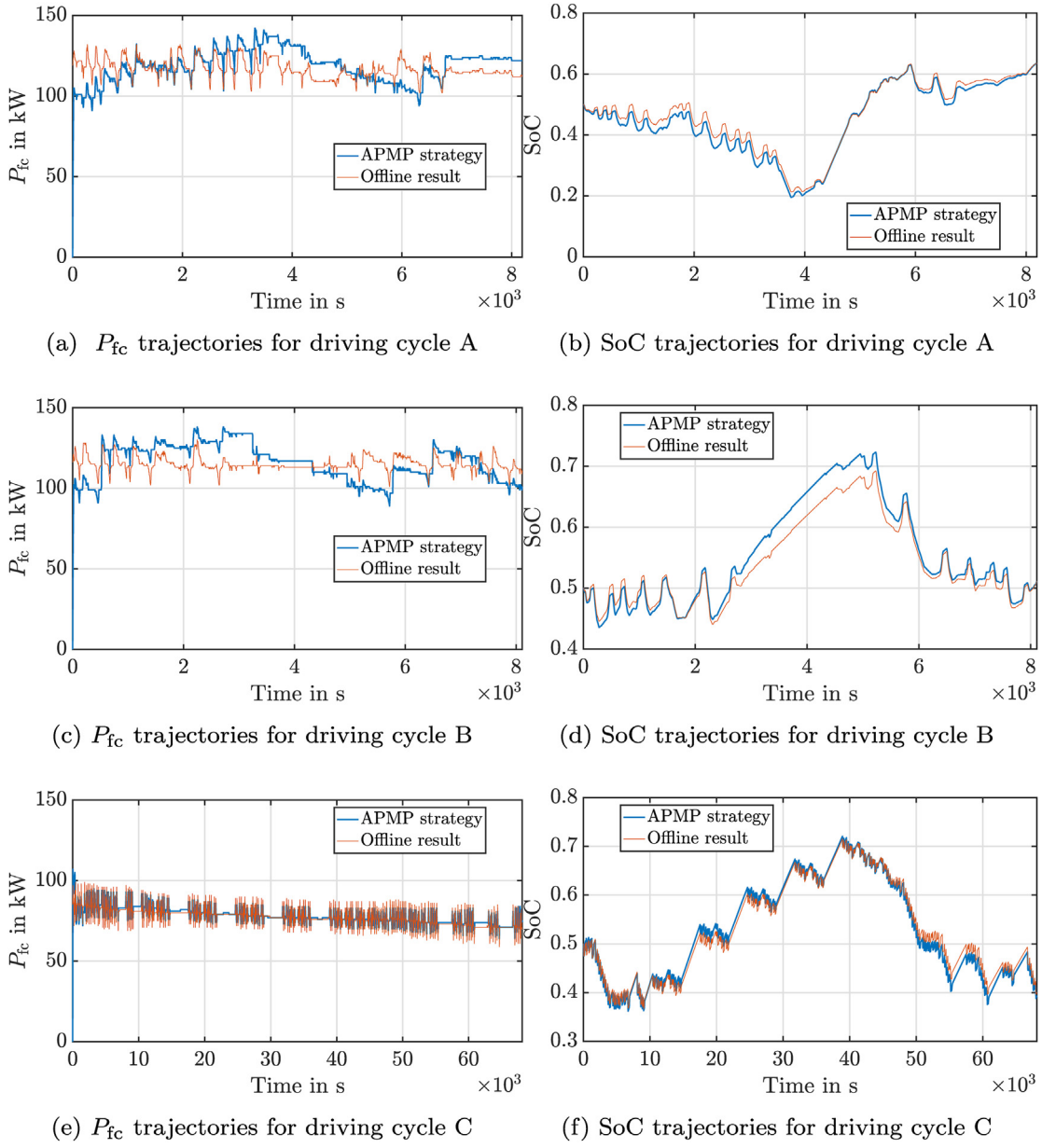

Fig. 15. SoC and the power trajectories of the fuel cell systems under the APMP-based strategies, together with the offline results.

maximal net power of 150 kW and a battery system with a rated charge and discharge current of 900 A. Instead of a real train, the load power demand for a half regional train is simulated using dSPACE SCALEXIO and realized with a dc/dc converter on the load side. A load unit is used to absorb the mean power of the fuel cell systems. A load battery system, which is the same as the battery system on the source side, is utilized to absorb the high peak power.

However, due to hardware's technical restrictions, the load battery system cannot cover the simulated maximal power. Therefore, the implemented load power on the load side is downscaled by one third, which is formulated as follows:

$$P_{\text{load,testbench}} = \frac{2}{3} \cdot P_{\text{load}} + \frac{1}{3} \cdot P_{\text{fc}}. \tag{19}$$

Here, one of the three parallel branches included in the battery system is turned off by software. Besides, the output power of the fuel cell systems is not downscaled to assure that the fuel economy validation of strategies is not influenced. Next, the battery power on the test bench is calculated as:

$$P_{\text{bat,testbench}} = P_{\text{load,testbench}} - P_{\text{fc}} = \frac{2}{3} \cdot \left(P_{\text{load}} - P_{\text{fc}} \right) \tag{20}$$

Furthermore, due to the same technical issues, a shortened driving cycle from Aachen to Cologne with 3065 s is utilized, which is half of the driving cycle B, as shown in Fig. 21. Additionally, the number of passengers in the half train is decreased from 120 to 60.

6.2. Experimental measurement results

Firstly, the correctness of modeling of the battery, the fuel cell system, the dc/dc converter, and the effectiveness of the offline PMP-based strategy as a benchmark are validated, which can also be found in Ref. [31]. Then, the effectiveness of the online strategies is validated through hardware-in-the-loop experiments.

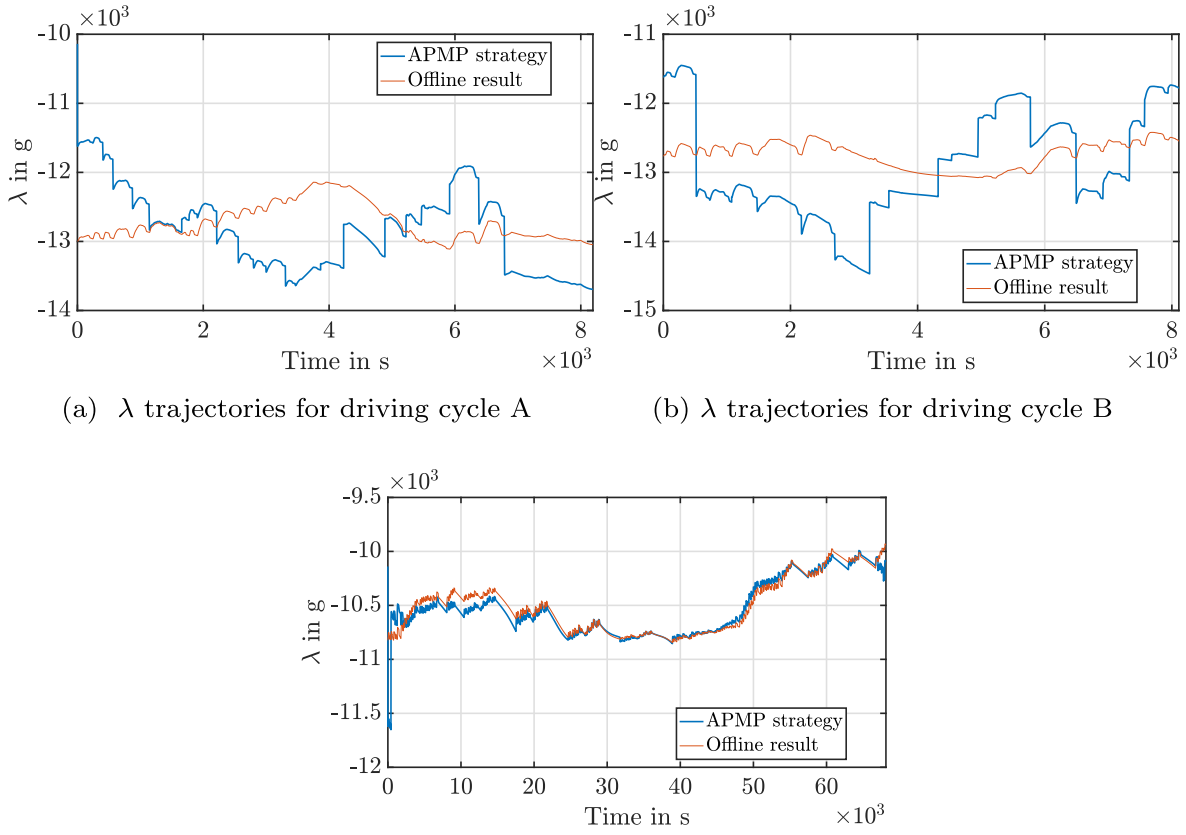

Fig. 16. Costate trajectories under the APMP strategy, compared to offline results.

As Fig. 22 shows, the experimentally measured trajectories follow the simulated signal trajectories. Moreover, the measured SoC values, which overlap with the simulated SoC values to a large degree, have a minimum scale of 1%. Based on the measured fuel cell power and SoC trajectories, the accuracy of the test bench is validated.The measured power trajectories of the fuel cell system and SoC under the adaptive rule-based strategy as well as the APMP strategy with and without considering the relaxation process in batteries are displayed with their corresponding offline results in Figs. 23–25, respectively. As a comparison, the corresponding offline PMP results, which use the same load trajectories and SoC boundary values as the online strategies to be validated, are added to the plots. It is observed that the measured output power trajectories of the fuel cell system maintain around the offline PMP results. Furthermore, the measured and offline calculated SoC trajectories are also highly overlapped.

Regarding the load follower strategy, due to the limitation of the maximal fuel cell power in the test bench, 150 kW, the strategy is also restrictively implemented. The resulted SoC trajectory still overlaps with the offline one, as displayed in Fig. 26. Furthermore, the SoC end value is much higher than the initial value, which does not satisfy the charge-sustaining condition, if the initial SoC equals to 0.5.The hydrogen consumption differences between the experimental and their corresponding offline results are listed in Table 5, which are 1.44%, 1.49%, 1.06%, and 1.87%, respectively. As the experimental results are pretty close to the offline PMP results, the hydrogen usage efficiency under the online strategies is validated. It deserves mentioning that the load follower strategy's performance is better than the developed adaptive rule-based strategy in the experiment measurement, and the reason lies in the shortened driving cycle. The APMP strategy, which does not consider the relaxation process in batteries, realizes the best fuel economy if the evaluations are based on comparison to the corresponding offline PMP results. However, suppose the measured hydrogen consumption under the two kinds of APMP strategies, with the relaxation process considered or not, is directly compared with the identical SoC end values. In that case, the total hydrogen consumption of the APMP strategy considering the relaxation process in batteries is 11366 g, which is 9 g lower than that of the APMP strategy without considering the relaxation processes. Accordingly, the measured hydrogen consumption of the APMP considering the relaxation process is the least and equals 161.9 g/km. Therefore, different evaluation criteria may lead to different conclusions due to the short driving cycle used for experimental testing. Nevertheless, the APMP performs better than the rule-based strategy and the load follower regarding the hydrogen efficiency and charge-sustaining condition.

7. Conclusions

In this contribution, a comparative study among four different scalable energy management strategies is investigated. For that purpose, the offline PMP strategy considering the relaxation process in batteries is proposed, which is used as an accurate and fair reference to evaluate the performance of different online strategies. After that, the principles and implementation of four scalable energy management strategies are introduced, including the load follower, the adaptive rule-based strategy, and the APMP strategy considering the relaxation process in batteries or not. From the load follower strategy to the APMP considering the relaxation processes

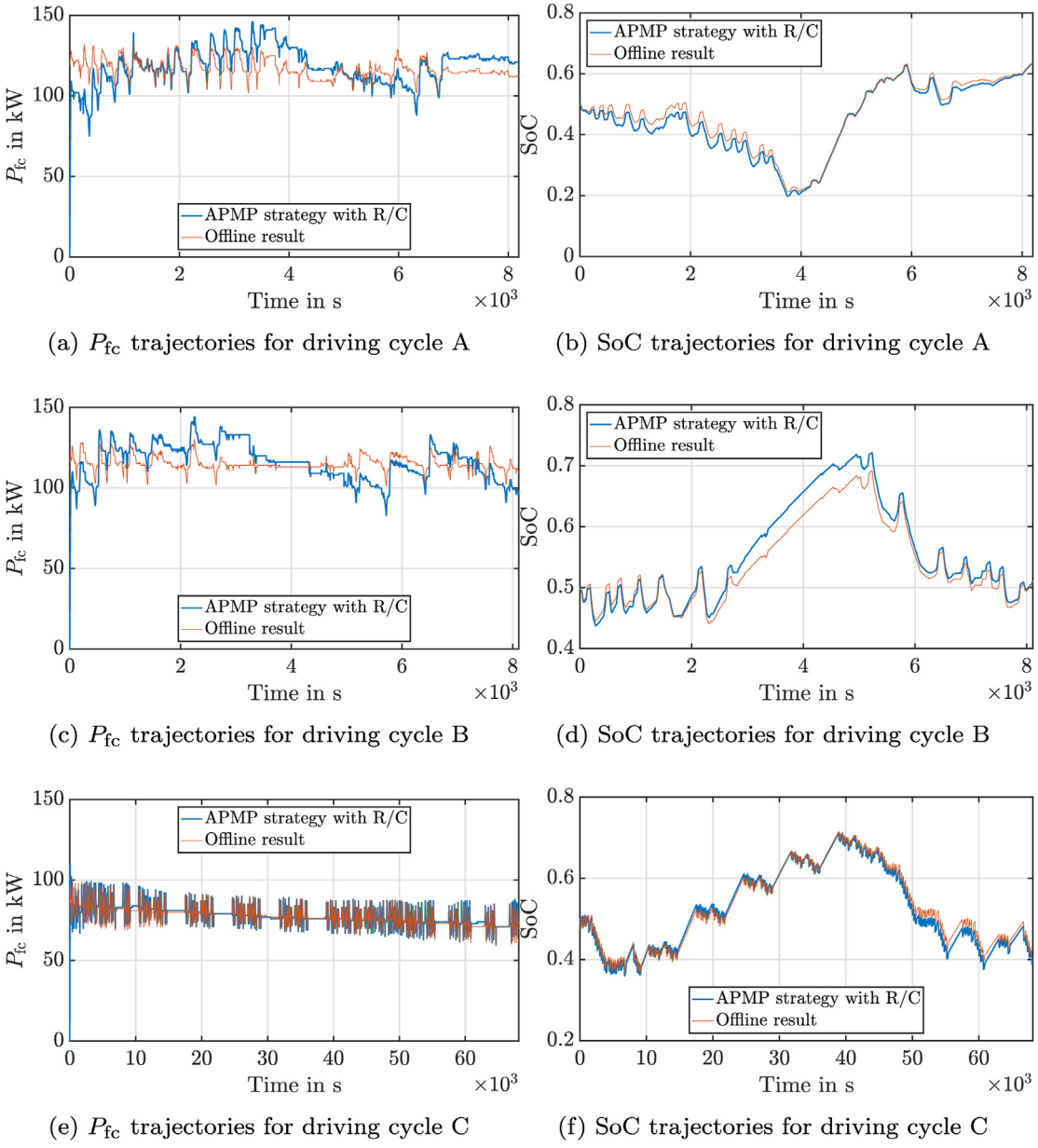

Fig. 17. SoC and the output power trajectories of the fuel cell system, under the APMP strategies with relaxation process considered, compared to offline PMP results.

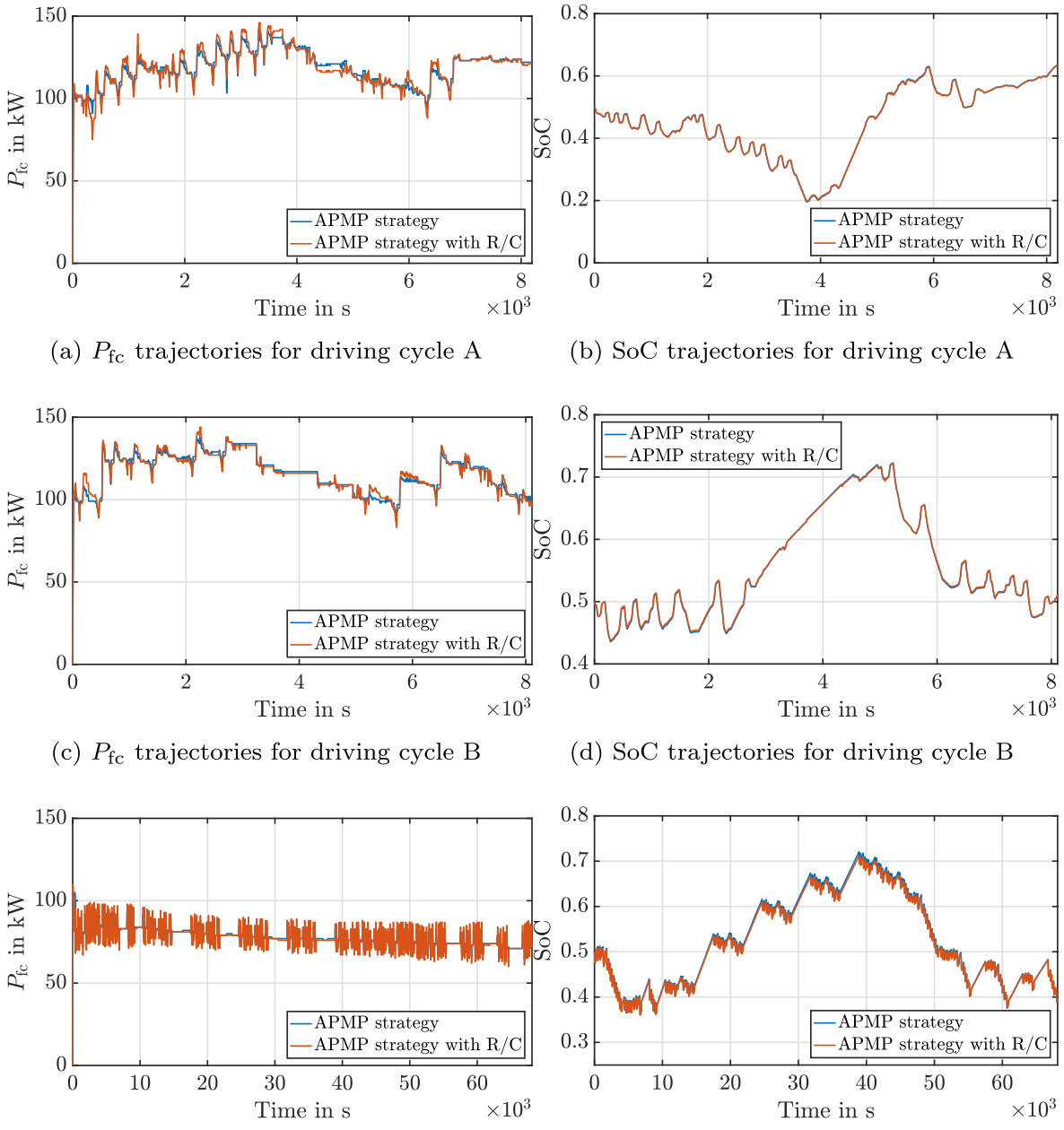

(a) P_{fc} trajectories for driving cycle A

(b) SoC trajectories for driving cycle A

(c) P_{fc} trajectories for driving cycle B

(d) SoC trajectories for driving cycle B

(e) P_{fc} trajectories for driving cycle C

(f) SoC trajectories for driving cycle C

Fig. 18. Simulation results under the APMP strategies with and without relaxation process considered.

Table 3
Simulation results of APMP strategies.

Driving cycle		A	B	C
APMP	P_{fc}	118.68	116.04	78.12
	SoC_{end}	0.636	0.512	0.403
	λ (g)	−12841	−12901	−10525
	m_{H_2} (g)	32736	31552	168856
	Offline m_{H_2} (g)	32042	31082	167816
	Ref. m_{H_2}	2.2 %	1.5 %	0.6 %
	m_{H_2} (g/km)	212.4	216.4	288.8
APMP with R/C	P_{fc}	118.44	115.95	78.09
	SoC_{end}	0.634	0.511	0.403
	λ (g)	−12829	−12891	−10517
	m_{H_2} (g)	32680	31522	168820
	Offline m_{H_2} (g)	32000	31078	167818
	Ref. m_{H_2}	2.1 %	1.4 %	0.6 %
	m_{H_2} (g/km)	212	216.2	288.8

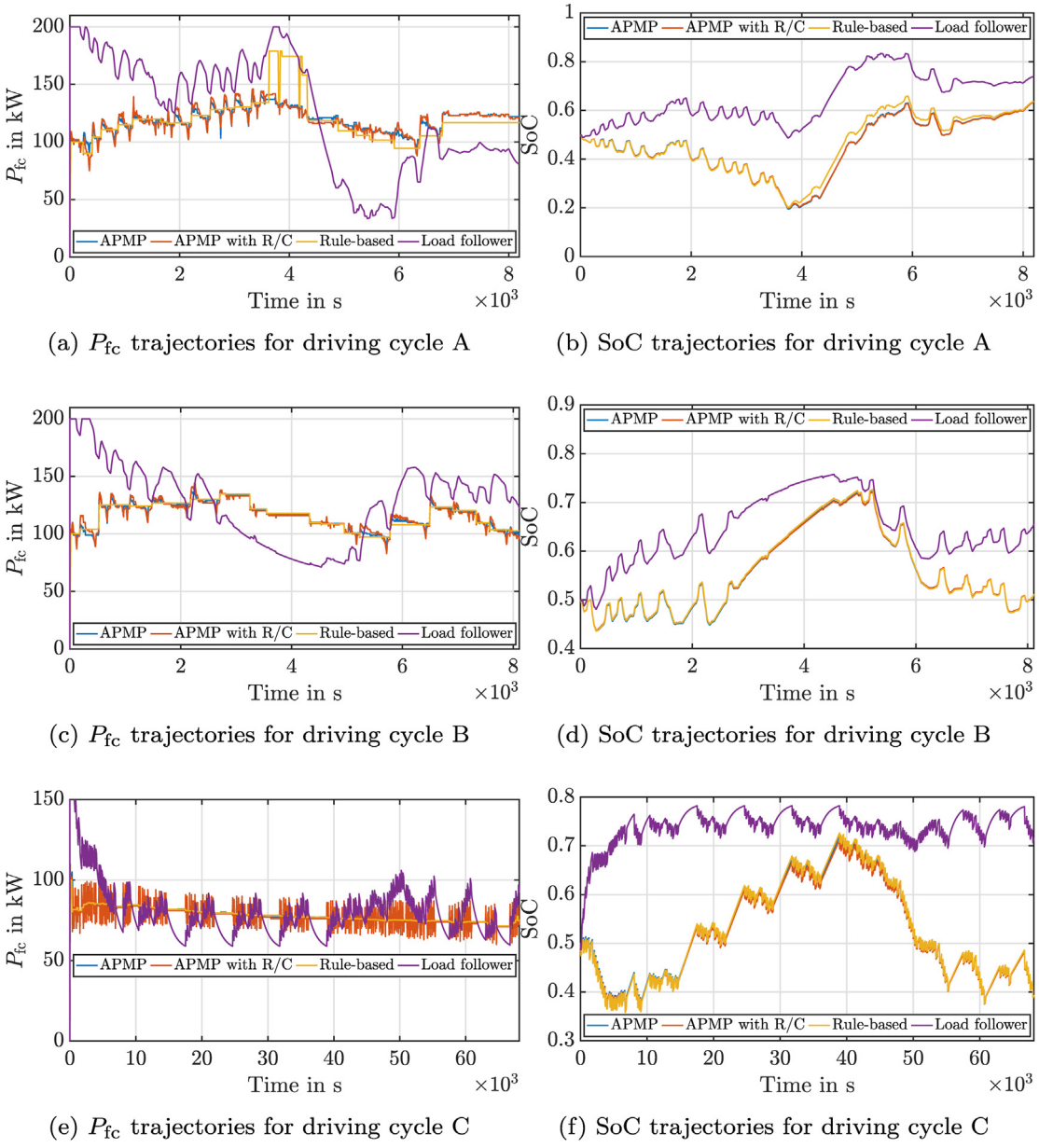

(a) P_{fc} trajectories for driving cycle A (b) SoC trajectories for driving cycle A

(c) P_{fc} trajectories for driving cycle B (d) SoC trajectories for driving cycle B

(e) P_{fc} trajectories for driving cycle C (f) SoC trajectories for driving cycle C

Fig. 19. Comparison of all strategies.

Table 4
Comparison of all strategies.

Driving cycle	Strategy	m_{H_2} (g)	m_{H_2} (g/km)	Ref. Offline
A	Load follower	37514	243.4	7.7 %
	Rule-based	33074	214.6	3.1 %
	APMP	32736	212.4	2.2 %
	APMP wich R/C	32680	212	2.1 %
B	Load follower	36346	249.2	4.2 %
	Rule-based	31590	216.6	1.6 %
	APMP	31552	216.4	1.5 %
	APMP wich R/C	31522	216.2	1.4 %
C	Load follower	177220	303.2	1.6 %
	Rule-based	168972	289	0.7 %
	APMP	168856	288.8	0.6 %
	APMP wich R/C	168820	288.8	0.6 %

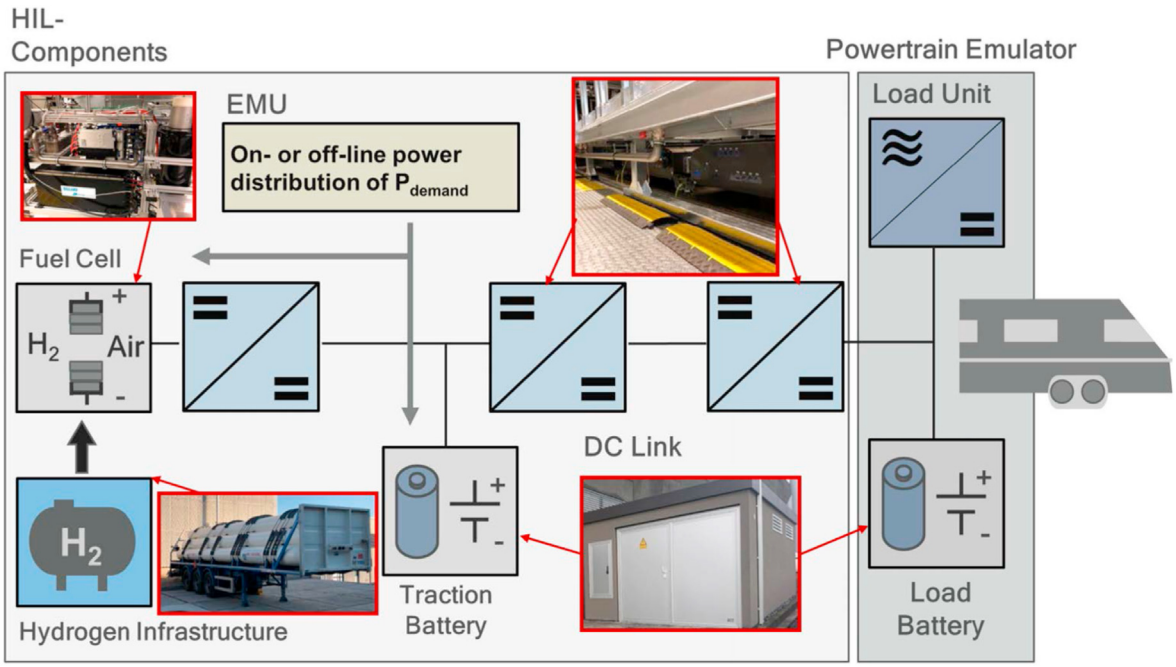

Fig. 20. Structure of the test bench with load power emulated at RWTH Aachen University.

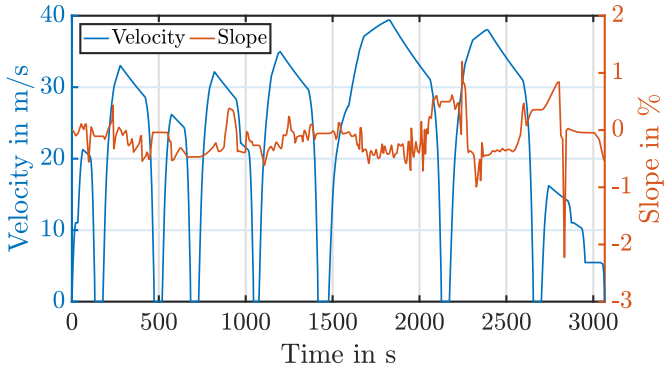

Fig. 21. The shortened driving cycle from Aachen to Cologne for measurement on test bench.

in batteries, increasingly accurate modeling is integrated into energy management strategies. They are compared firstly based on simulation and then on experimental measurement. It is worth mentioning that this comparative study is focused on scalable strategies, which has not been found in other works so far. Regarding the comparison results, under a typical whole-day driving cycle of regional trains, more consumption of 1.6%, 0.7%, 0.6%, and 0.6% compared to the offline results are observed. After test bench measurement, the APMP strategy considering the relaxation process in batteries consumes the least hydrogen per kilometer travel of 161.9 g/km, with charge sustaining maintained. Therefore, the APMP strategy with the most precise modeling of batteries and fuel cells utilized achieves the best hydrogen efficiency. It is suggested that the energy strategy should be chosen based on the available modeling accuracy to maximize fuel economy and fuel cell lifetime. In the future, the mean value of the fuel cell power can be calculated more accurately by considering the future geographic and load information, which can be provided by using GPS and communication methods.

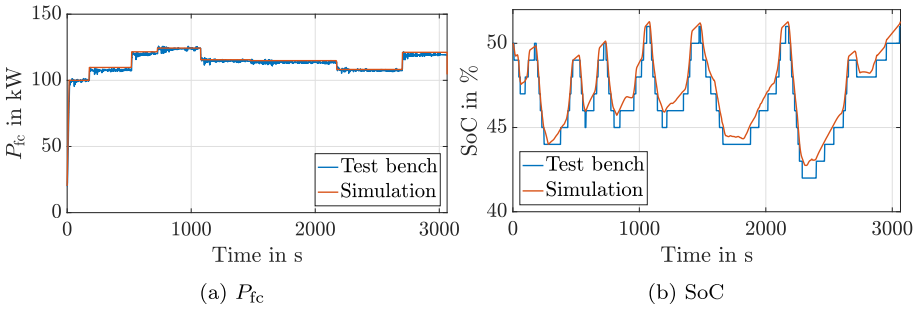

(a) P_{fc} (b) SoC

Fig. 22. Measured and simulated results under the adaptive rule-based strategies.

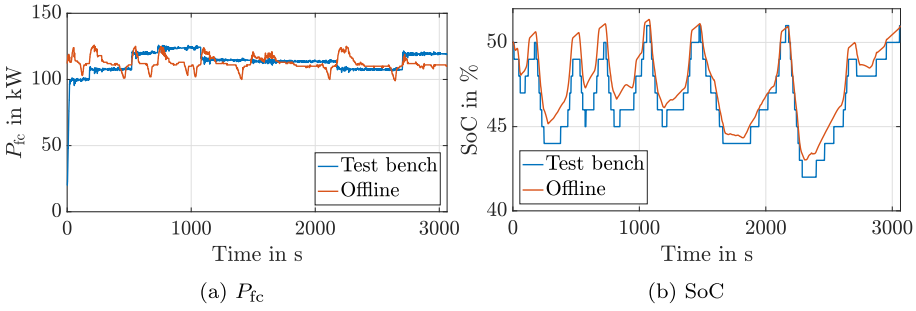

(a) P_{fc} (b) SoC

Fig. 23. Measured SoC and fuel cell power trajectories under the adaptive rule-based strategies, together with the corresponding offline PMP results.

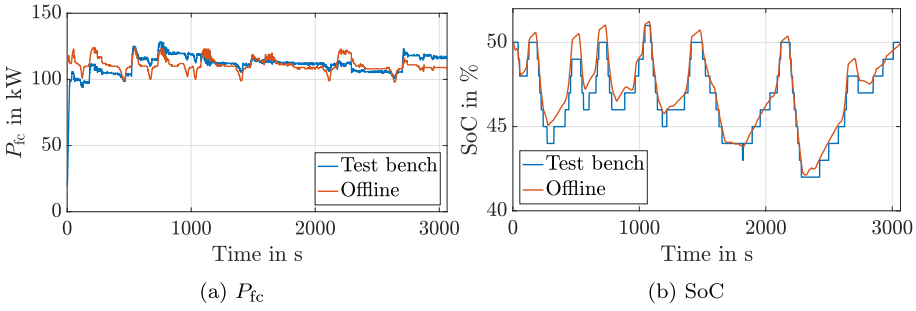

(a) P_{fc} (b) SoC

Fig. 24. Measured SoC and fuel cell power trajectories under the APMP-based strategies, together with the corresponding offline PMP results.

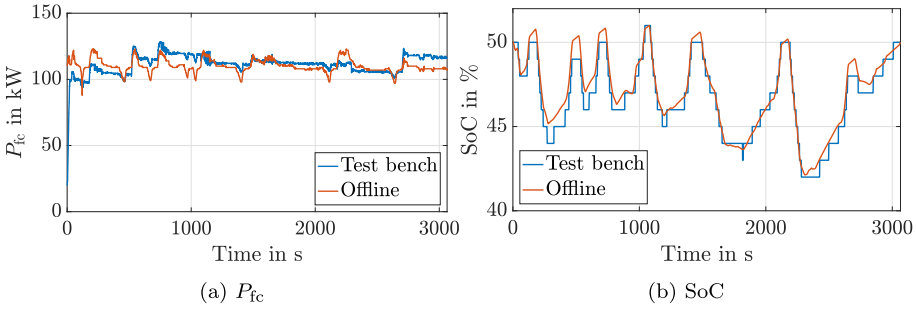

(a) P_{fc} (b) SoC

Fig. 25. Measured SoC and fuel cell power trajectories under the APMP strategy with relaxation considered, together with the corresponding offline PMP results.

CRediT authorship contribution statement

Hujun Peng: Conceptualization, Methodology, Formal analysis, Validation, Writing – original draft. **Zhu Chen:** Software, Data curation, Writing – original draft. **Kai Deng:** Writing – review & editing, Validation. **Steffen Dirkes:** Writing – review & editing. **Cem Ünlübayir:** Writing – review & editing. **Andreas Thul:** Writing – review & editing, Project administration. **Lars Löwenstein:** Resources, Writing – review & editing. **Dirk Uwe Sauer:** Funding acquisition, Writing – review & editing. **Stefan**

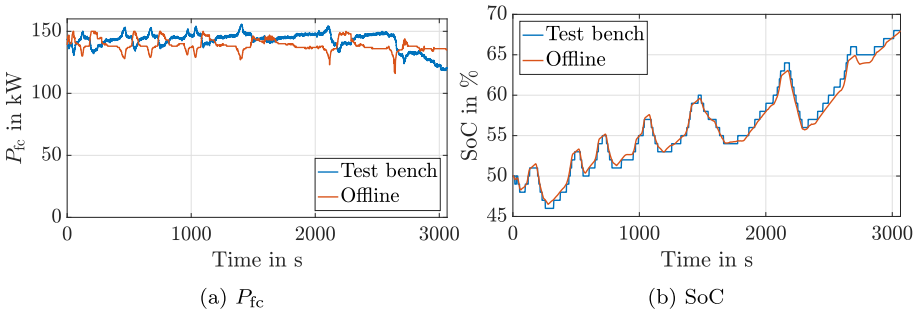

Fig. 26. Measured results of load follower in the test bench with the corresponding offline results.

Table 5
Measured results of all strategies in the test bench.

Strategy	Load follower	Rule-based	APMP	APMP-R/C
-				
P_{fc} (kW)	142.3	114.8	112.9	112.3
SoC_{end}	0.69	0.51	0.50	0.50
Measured m_{H_2} (g)	15362	11606	11375	11366
Offline m_{H_2} (g)	15144	11436	11256	11157
Ref. m_{H_2} to offline	1.44 %	1.49 %	1.06 %	1.87 %
m_{H_2}(full train) (g/km)	218.8	165.3	162	161.9

Pischinger: Funding acquisition, Writing – review & editing. **Kay Hameyer:** Supervision, Funding acquisition, Writing – review & editing.

Declaration of competing interest

The authors declare that they have no known competing financial interests or personal relationships that could have appeared to influence the work reported in this paper.

References

[1] European commission unveils its hydrogen strategy. https://fuelcellsworks.com/news/european-commission-unveils-its-hydrogen-strategy/. [Accessed 29 January 2021].

[2] Second generation mirai. https://www.toyota-europe.com/world-of-toyota/articles-news-events/2019/new-mirai-concept. [Accessed 29 January 2021].

[3] Europe's largest hybrid fuel cell bus fleet and first hydrogen infrastructure for public transport unveiled. https://fuelcellsworks.com/news/europes-largest-hybrid-fuel-cell-bus-fleet-and-first-hydrogen-infrastructure-for-public-transport-unveiled/. [Accessed 29 January 2021].

[4] World's first hydrogen train coradia ilint honoured. https://www.alstom.com/solutions/rolling-stock/coradia-ilint-worlds-1st-hydrogen-powered-train. [Accessed 29 January 2021].

[5] Development and validation of a high-performance fuel cell drive for hybrid emu trains in a traction modular system. https://www.now-gmbh.de/en/projectfinder/x-emu/. [Accessed 29 January 2021].

[6] Deutsche bahn, siemens launch hydrogen trains trial. https://www.dw.com/en/deutsche-bahn-siemens-launch-hydrogen-trains-trial/a-55716107. [Accessed 29 January 2021].

[7] Li H, Chaoui H, Gualous H. Cost minimization strategy for fuel cell hybrid electric vehicles considering power sources degradation. IEEE Trans Veh Technol 2020;69(11):12832–42. https://doi.org/10.1109/TVT.2020.3031000.

[8] Yue M, Jemei S, Gouriveau R, Zerhouni N. Review on health-conscious energy management strategies for fuel cell hybrid electric vehicles: degradation models and strategies. Int J Hydrogen Energy 2019;44(13):6844–61.

[9] Li W, Cui H, Nemeth T, Jansen J, Ünlübayir C, Wei Z, Zhang L, Wang Z, Ruan J, Dai H, Wei X, Sauer DU. Deep reinforcement learning-based energy management of hybrid battery systems in electric vehicles. J. Energy Storage 2021;36:102355. https://doi.org/10.1016/j.est.2021.102355. https://www.sciencedirect.com/science/article/pii/S2352152X21001158.

[10] Teng T, Zhang X, Dong H, Xue Q. A comprehensive review of energy management optimization strategies for fuel cell passenger vehicle. Int J Hydrogen Energy 2020;45(39):20293–303. https://doi.org/10.1016/j.ijhydene.2019.12.202. https://www.sciencedirect.com/science/article/pii/S0360319920300057.

[11] İnci M, Büyük M, Demir MH, İlbey G. A review and research on fuel cell electric vehicles: topologies, power electronic converters, energy management methods, technical challenges, marketing and future aspects. Renew Sustain Energy Rev 2021;137:110648. https://doi.org/10.1016/j.rser.2020.110648. http://www.sciencedirect.com/science/article/pii/S1364032120309321.

[12] Wang Y, Wang L, Li M, Chen Z. A review of key issues for control and management in battery and ultra-capacitor hybrid energy storage systems. eTransportation 2020;4:100064. https://doi.org/10.1016/j.etran.2020.100064. https://www.sciencedirect.com/science/article/pii/S2590116820300217.

[13] Wang Y, Sun Z, Li X, Yang X, Chen Z. A comparative study of power allocation strategies used in fuel cell and ultracapacitor hybrid systems. Energy 2019;189:116142. https://doi.org/10.1016/j.energy.2019.116142. https://www.sciencedirect.com/science/article/pii/S0360544219318377.

[14] Soumeur MA, Gasbaoui B, Abdelkhalek O, Ghouili J, Toumi T, Chakar A. Comparative study of energy management strategies for hybrid proton exchange membrane fuel cell four wheel drive electric vehicle. J Power Sources 2020;462:228167. https://doi.org/10.1016/j.jpowsour.2020.228167. http://www.sciencedirect.com/science/article/pii/S0378775320304705.

[15] Lü X, Wu Y, Lian J, Zhang Y, Chen C, Wang P, Meng L. Energy management of hybrid electric vehicles: a review of energy optimization of fuel cell hybrid power system based on genetic algorithm. Energy Convers Manag 2020;205:112474.

[16] Chen H, Zhang Z, Guan C, Gao H. Optimization of sizing and frequency control in battery/supercapacitor hybrid energy storage system for fuel cell ship. Energy 2020:117285.

[17] Wang Y, Sun Z, Chen Z. Energy management strategy for battery/supercapacitor/fuel cell hybrid source vehicles based on finite state machine. Appl Energy 2019;254:113707.

[18] Gharibeh HF, Yazdankhah AS, Azizian MR. Energy management of fuel cell electric vehicles based on working condition identification of energy storage systems, vehicle driving performance, and dynamic power factor. J. Energy Storage 2020;31:101760. https://doi.org/10.1016/j.est.2020.101760. https://www.sciencedirect.com/science/article/pii/S2352152X20315978.

[19] Wu X, Hu X, Yin X, Peng Y, Pickert V. Convex programming improved online power management in a range extended fuel cell electric truck. J Power Sources 2020;476:228642. https://doi.org/10.1016/j.jpowsour.2020.228642. http://www.sciencedirect.com/science/article/pii/S0378775320309460.

[20] Kandidayeni M, Macias Fernandez AO, Khalatbarisoltani A, Boulon L, Kelouwani S, Chaoui H. An online energy management strategy for a fuel cell/battery vehicle considering the driving pattern and performance drift impacts. IEEE Trans Veh Technol 2019;68(12):11427–38. https://doi.org/10.1109/TVT.2019.2936713.

[21] Rezaei A, Burl JB, Zhou B. Estimation of the ecms equivalent factor bounds for hybrid electric vehicles. IEEE Trans Contr Syst Technol 2017;26(6):2198–205.

[22] Song K, Wang X, Li F, Sorrentino M, Zheng B. Pontryagin's minimum principle-based real-time energy management strategy for fuel cell hybrid electric vehicle considering both fuel economy and power source durability. Energy 2020:118064.

[23] Wang T, Li Q, Wang X, Qiu Y, Liu M, Meng X, Li J, Chen W. An optimized energy management strategy for fuel cell hybrid power system based on maximum efficiency range identification. J Power Sources 2020;445:227333. https://doi.org/10.1016/j.jpowsour.2019.227333. http://www.sciencedirect.com/science/article/pii/S0378775319313266.

[24] Song K, Ding Y, Hu X, Xu H, Wang Y, Cao J. Degradation adaptive energy management strategy using fuel cell state-of-health for fuel economy improvement of hybrid electric vehicle. Appl Energy 2021;285:116413. https://doi.org/10.1016/j.apenergy.2020.116413. http://www.sciencedirect.com/science/article/pii/S0306261920317803.

[25] Li X, Wang Y, Yang D, Chen Z. Adaptive energy management strategy for fuel cell/battery hybrid vehicles using pontryagin's minimal principle. J Power Sources 2019;440:227105.

[26] He H, Quan S, Sun F, Wang Y. Model predictive control with lifetime constraints based energy management strategy for proton exchange membrane fuel cell hybrid power systems. IEEE Trans Ind Electron 2020;67(10):9012–23. https://doi.org/10.1109/TIE.2020.2977574.

[27] Zhou Y, Ravey A, Péra M-C. Real-time cost-minimization power-allocating

strategy via model predictive control for fuel cell hybrid electric vehicles. Energy Convers Manag 2021;229:113721. https://doi.org/10.1016/j.enconman.2020.113721. http://www.sciencedirect.com/science/article/pii/S0196890420312450.

[28] Zhou Y, Ravey A, Péra M-C. Multi-objective energy management for fuel cell electric vehicles using online-learning enhanced markov speed predictor. Energy Convers Manag 2020;213:112821. https://doi.org/10.1016/j.enconman.2020.112821. http://www.sciencedirect.com/science/article/pii/S0196890420303599.

[29] Deng K, Peng H, Dirkes S, Gottschalk J, Ünlübayir C, Thul A, Löwenstein L, Pischinger S, Hameyer K. An adaptive pmp-based model predictive energy management strategy for fuel cell hybrid railway vehicles. eTransportation 2021;7:100094. https://doi.org/10.1016/j.etran.2020.100094. http://www.sciencedirect.com/science/article/pii/S2590116820300527.

[30] Peng H, Li J, Löwenstein L, Hameyer K. A scalable, causal, adaptive energy management strategy based on optimal control theory for a fuel cell hybrid railway vehicle. Appl Energy 2020;267:114987.

[31] H. Peng, Z. Chen, J. Li, K. Deng, S. Dirkes, J. Gottschalk, C. Ünlübayir, A. Thul, L. Löwenstein, S. Pischinger, et al., Offline optimal energy management strategies considering high dynamics in batteries and constraints on fuel cell system power rate: from analytical derivation to validation on test bench, Appl Energy 282 116152.

[32] Tran D-D, Vafaeipour M, El Baghdadi M, Barrero R, van Mierlo J, Hegazy O. Thorough state-of-the-art analysis of electric and hybrid vehicle powertrains: topologies and integrated energy management strategies. Renew Sustain Energy Rev 2020;119:109596. https://doi.org/10.1016/j.rser.2019.109596. http://www.sciencedirect.com/science/article/pii/S1364032119308044.

[33] Sun H, Fu Z, Tao F, Zhu L, Si P. Data-driven reinforcement-learning-based hierarchical energy management strategy for fuel cell/battery/ultracapacitor hybrid electric vehicles. J Power Sources 2020;455:227964.

[34] Peng H, Li J, Thul A, Deng K, Ünlübayir C, Löwenstein L, Hameyer K. A scalable, causal, adaptive rule-based energy management for fuel cell hybrid railway vehicles learned from results of dynamic programming. eTransportation 2020:100057.

[35] Peng H, Cao H, Dirkes S, Chen Z, Deng K, Gottschalk J, Ünlübayir C, Thul A, Löwenstein L, Sauer DU, Pischinger S, Hameyer K. Validation of robustness and fuel efficiency of a universal model-based energy management strategy for fuel cell hybrid trains: from analytical derivation via simulation to measurement on test bench. Energy Convers Manag 2021;229:113734. https://doi.org/10.1016/j.enconman.2020.113734. http://www.sciencedirect.com/science/article/pii/S0196890420312589.